

# Shape of Thought: Progressive Object Assembly via Visual Chain-of-Thought

Yu Huo<sup>\*1,2,3</sup> Siyu Zhang<sup>\*1,2,3</sup> Kun Zeng<sup>\*4</sup> Haoyue Liu<sup>1</sup> Owen Lee<sup>5</sup> Junlin Chen<sup>1</sup> Yuquan Lu<sup>3</sup> Yifu Guo<sup>4</sup>  
Yaodong Liang<sup>6</sup> Xiaoying Tang<sup>1,2,3</sup>

## Abstract

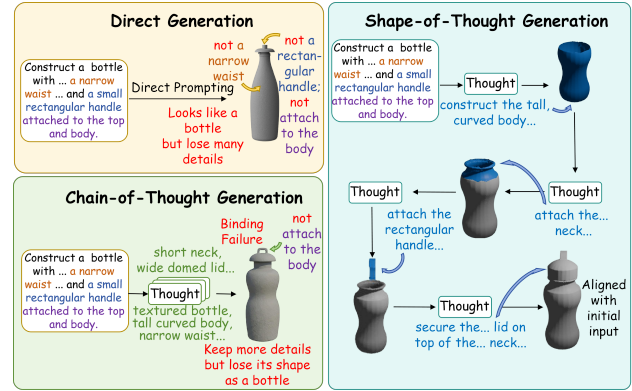
Multimodal models for text-to-image generation have achieved strong visual fidelity, yet they remain brittle under compositional structural constraints—notably generative numeracy, attribute binding, and part-level relations. To address these challenges, we propose **Shape-of-Thought (SoT)**, a visual CoT framework that enables *progressive shape assembly via coherent 2D projections* without external engines at inference time. SoT trains a unified multimodal autoregressive model to generate interleaved textual plans and rendered intermediate states, helping the model capture shape-assembly logic without producing explicit geometric representations. To support this paradigm, we introduce **SoT-26K**, a large-scale dataset of grounded assembly traces derived from part-based CAD hierarchies, and **T2S-CompBench**, a benchmark for evaluating structural integrity and trace faithfulness. Fine-tuning on SoT-26K achieves 88.4% on component numeracy and 84.8% on structural topology, outperforming text-only baselines by around 20%. SoT establishes a new paradigm for transparent, process-supervised compositional generation. The code is available at <https://anonymous.4open.science/r/16FE/>. The SoT-26K dataset will be released upon acceptance.

## 1. Introduction

Chain-of-Thought (CoT) prompting has fundamentally enhanced complex reasoning by eliciting intermediate ratio-

<sup>1</sup>School of Science and Engineering, The Chinese University of Hong Kong, Shenzhen <sup>2</sup>The Shenzhen Institute of Artificial Intelligence and Robotics for Society <sup>3</sup>Guangdong Provincial Key Laboratory of Future Networks of Intelligence <sup>4</sup>Sun Yat-sen University <sup>5</sup>School of Data Science, The Chinese University of Hong Kong, Shenzhen <sup>6</sup>The Hong Kong University of Science and Technology, Guangzhou. Correspondence to: Xiaoying Tang <tangxiaoying@cuhk.edu.cn>.

Preprint. January 30, 2026.



**Figure 1. Comparison of generation paradigms.** While direct generation fails to capture details and text-based CoT leads to semantic binding failures, SoT improves structural compliance on our tasks. By decomposing complex prompts into sequential visual sub-goals, SoT corrects structural deficiencies and ensures the final output aligns with the text description.

nales instead of relying on direct outputs (Wei et al., 2022; Wang et al., 2023). In multimodal settings, augmenting these traces with “visual thoughts” provides a powerful mechanism for spatial planning, effectively serving as a **visual working memory** (Yao et al., 2023; Li et al., 2025).

However, 2D generators remain brittle under compositional structural constraints, notably generative numeracy, attribute binding, and part-level relations. They often hallucinate counts or omit repeated thin structures when prompts demand fine-grained structural depiction. (Ho et al., 2020; Deng et al., 2025) Meanwhile, text-only CoT can expand reasoning traces but still lacks visual grounding, making it hard to verify and correct structural drift along the generation trajectory. These failure modes naturally extend to text-to-3D pipelines: many modern systems are driven by image-space priors and rendered-view supervision, so compositional ambiguities and errors in the 2D guidance signal can manifest as missing parts, wrong numeracy, or inconsistent relations in the resulting 3D outputs. (Hong et al., 2024) As illustrated in Figure 1, our method addresses these issues by decomposing synthesis into a visible, verifiable trace with step-wise visual grounding.

To bridge this gap, we propose **Shape-of-Thought (SoT)**,

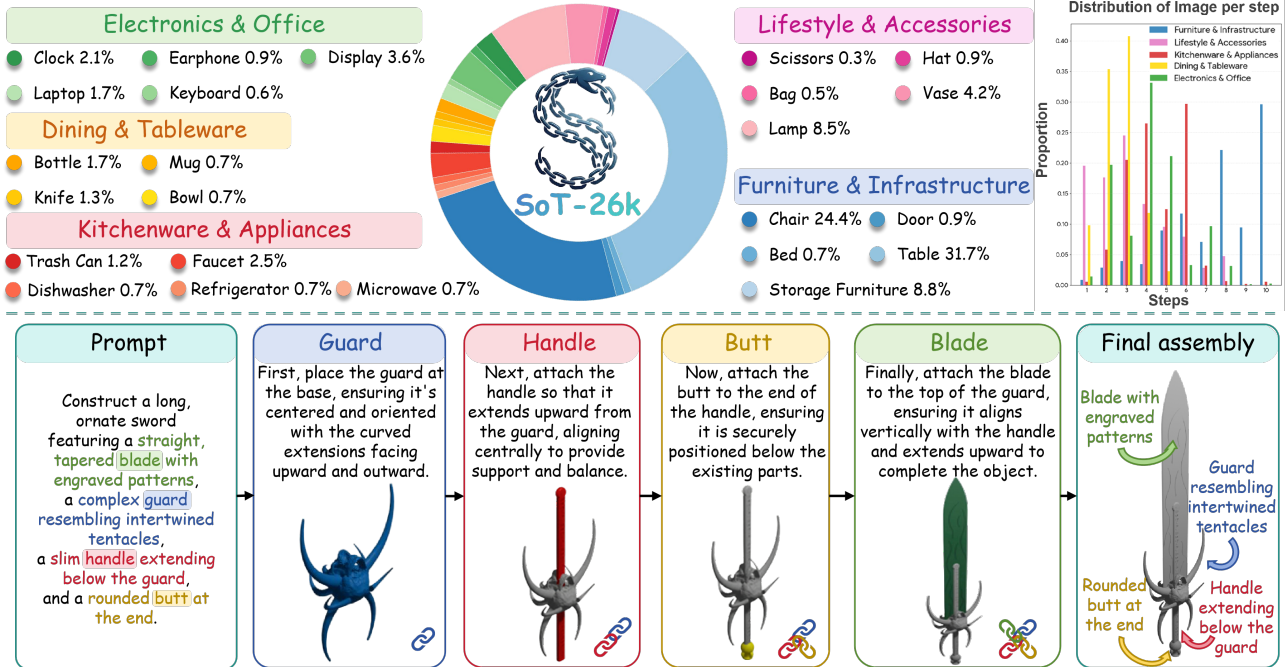


Figure 2. **Overview of the SoT Ecosystem.** Top: Statistics of the proposed SoT-26K dataset, showing the distribution of object categories and assembly step lengths. The data covers a wide range of structural complexities, from simple short-horizon objects to complex long-horizon assemblies. Bottom: The inference workflow of the SoT framework. Conditioned on a global goal prompt, the model autoregressively generates an interleaved multimodal trace, alternating between textual rationales and rendered intermediate states.

a framework for **progressive shape assembly that operates in the 2D rendered domain**. Unlike tool-augmented systems that rely on external engines, SoT trains a single early-fusion multimodal Transformer to generate an interleaved *text-image* trace. At each step, the model predicts a structural operation (rationale) and immediately grounds it by generating the resulting rendered state. This allows the model to “see” its own progress, providing step-wise visual feedback that promotes visual consistency.

To enable this paradigm, we construct a pipeline converting PartNet CAD assets (Mo et al., 2019) into step-aligned multimodal supervision. This yields **SoT-26K**, a large-scale dataset of 26K interleaved assembly traces, and supports **T2S-CompBench**, a benchmark that covers key aspects for evaluating structural integrity and trace faithfulness.

As shown in Figure 2, our contributions are three-fold:

- **Shape-of-Thought (SoT):** A visual Chain-of-Thought framework that decomposes shape assembly into sequential 2D visual sub-goals, enabling a single autoregressive model to capture structure-aware compositional regularities induced by part-based CAD supervision, without explicit 3D representations.
- **SoT-26K & T2S-CompBench:** A large-scale dataset of 26K grounded assembly traces with an automated

generation pipeline, paired with a hybrid benchmark combining VLM semantic judging and geometric mask stability for evaluating progressive shape assembly.

- **Empirical Validation:** Comprehensive experiments demonstrating that explicit visual grounding yields +24% improvement in component numeracy and +19% in structural topology over direct generation baselines.

## 2. Related Work

**From Direct Generation to Interleaved Multimodal Reasoning.** Text-to-image diffusion models can generate high-quality images from a single prompt (Ho et al., 2020; Dosovitskiy et al., 2021; Ramesh et al., 2022; Saharia et al., 2022; Rombach et al., 2022), yet often struggle with fine-grained compositional constraints, especially attribute binding and spatial relations. In language modeling, Chain-of-Thought prompting suggests that eliciting intermediate reasoning steps can improve compositional generalization (Wei et al., 2022; Lyu et al., 2023; Wang & Zhou, 2024). Recent multimodal extensions similarly externalize intermediate *visual thoughts*, generating images as part of the reasoning trace to support spatial working memory (Chen et al., 2024; Cheng et al., 2025; Gu et al., 2025; Tang et al., 2023; Zhong et al., 2025; Zhao et al., 2025; Dong et al., 2025; Tian et al., 2025;

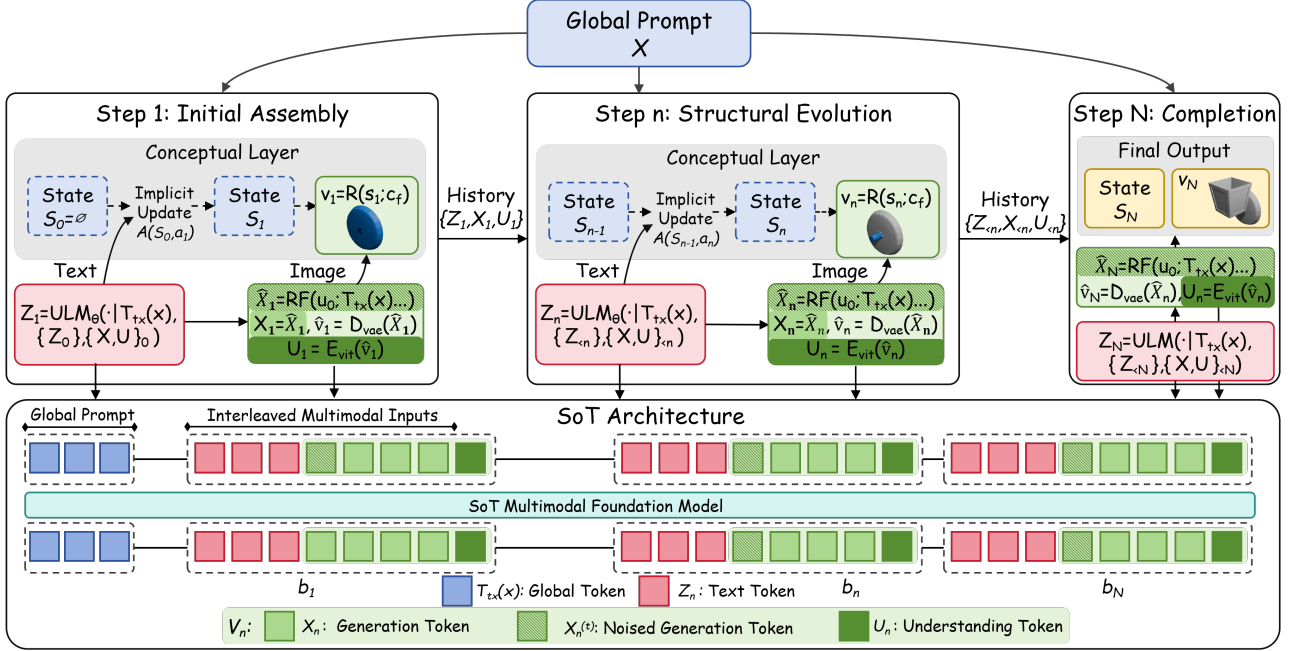


Figure 3. **Overview of the SoT framework.** The architecture progressively evolves from *Initial Assembly* to *Structural Evolution* and *Completion*. At each step  $n$ , the model utilizes a **Conceptual Layer** where textual rationales ( $z_n$ ) serve as a scaffold to guide the generation of grounded visual tokens ( $v_n$ ). The bottom panel illustrates the tokenization implementation, where interleaved text and vision tokens are processed by a unified multimodal foundation model.

Li et al., 2025; Wang et al., 2025). In parallel, early-fusion token-based models interleave text and image tokens within a single autoregressive stream, making mixed-modal traces a native output format (Yu et al., 2023; Team, 2025). Building on this paradigm, we study *process-supervised generation*, where the model outputs an interleaved text–image trace of intermediate assembly states, enabling step-wise supervision beyond direct generated images.

**Compositional Benchmarks and Assets.** Benchmarks such as T2I-CompBench++ provide controlled prompts to diagnose compositional failures in text-to-image generation, including attribute binding, spatial relations, numeracy, and complex compositions (Huang et al., 2025). Separately, PartNet offers large-scale 3D objects with fine-grained hierarchical part annotations (Mo et al., 2019). However, compositional T2I benchmarks typically supervise only the final image, while part-based 3D assets lack language-aligned, step-wise 2D traces suitable for training process-aware generators. Prior work leverages 3D either at inference time via tool-augmented systems (Yuan et al., 2024; Yamada et al., 2025; Tang et al., 2025) or by injecting 3D representations for grounded reasoning (Hong et al., 2023; Linghu et al., 2025; Cha & Kim, 2025). By contrast, we use part-based 3D structure to *synthesize step-aligned supervision in 2D image space*, pairing rendered intermediate assembly states with textual rationales.

## 3. Methodology

### 3.1. Shape-of-Thought

**Problem formulation.** Given a goal prompt  $x$  describing a target object, Shape-of-Thought (SoT) reframes text-conditioned shape generation from direct appearance synthesis into *progressive assembly*. Rather than producing a final image directly, the model generates an interpretable multimodal trace that alternates between (i) a textual decision describing an incremental construction action and (ii) a rendered intermediate state that grounds this decision and enables step-wise visual checking. At each step  $n \in \{1, \dots, N\}$ , where  $N$  is the number of assembly steps, the model outputs a textual plan  $z_n$  followed by a rendered observation  $v_n$ . **Formally, we treat shape assembly as a sequence of view-consistent 2D generation steps.**

**State and rendering.** Let  $s_n$  denote the abstract assembly state after  $n$  steps, with  $s_0 = \emptyset$ . In our dataset construction,  $s_n$  is realized by composing part-based CAD assets according to a deterministic schedule (fine-grained assembly scheduling; Sec. 3.2). Crucially, SoT does *not* require predicting explicit 3D geometry during generation: the model never observes meshes, point clouds, or part poses. We use  $s_n$  only for trace construction and evaluation, and never expose it to the model. The model only observes the state

through a fixed 2D rendering function:

$$v_n = \mathcal{R}(s_n; \mathbf{c}_f), \quad (1)$$

where  $\mathcal{R}$  is our Blender rendering protocol and  $\mathbf{c}_f$  is a canonical **front** camera. Using a canonical view reduces viewpoint ambiguity and stabilizes the tokenized sequence length. Our data additionally includes auxiliary renderings under fixed **left/right/back** cameras  $\{\mathbf{c}_l, \mathbf{c}_r, \mathbf{c}_b\}$  to support future multi-view grounding, although SoT in this paper operates in the single-view setting. Under this formulation,  $s_n$  serves as the *abstract structural ground truth*, while  $v_n$  provides the necessary *geometric evidence* for the model.

**Interleaved supervision.** Each example provides a step-aligned interleaved trace

$$\mathcal{T} = \{(z_1, v_1), (z_2, v_2), \dots, (z_N, v_N)\}, \quad (2)$$

where  $z_n$  specifies the incremental action at step  $n$  (e.g., which part is added and how it attaches to the existing structure), and  $v_n$  is the rendered consequence of that action. Conceptually, the underlying assembly evolves via an atomic action  $a_n$  (part selection with placement/attachment):

$$s_n = \mathcal{A}(s_{n-1}, a_n), \quad s_0 = \emptyset, \quad (3)$$

where  $\mathcal{A}$  is the deterministic assembly operator used only during data generation. This coupling yields **mutual disambiguation**: language resolves *what* to construct and why, whereas vision resolves *where/how* the new component fits, providing explicit grounding that text-only CoT lacks.

**Token-level formulation.** We serialize each example into a unified token stream that interleaves *text tokens* and *image-token blocks*. Let  $T_{\text{tx}}(\cdot)$  be the text tokenizer. Following the Bagel design (Deng et al., 2025), each rendered image  $v_n$  is represented by an image-token block that bundles (i) *understanding tokens* from a ViT encoder and (ii) *generation tokens* in a frozen VAE (Kingma & Welling, 2013) latent space. During training, we also sample a continuous rectified-flow time and construct the noised latents along the linear path from data to noise, where  $t_n = 0$  corresponds to clean data and  $t_n = 1$  to pure noise. Concretely,

$$Z_n = T_{\text{tx}}(z_n), \quad (4)$$

$$U_n = E_{\text{vit}}(v_n), \quad (5)$$

$$X_n = E_{\text{vae}}(v_n), \quad (6)$$

$$\tilde{X}_n^{(t_n)} = (1 - t_n)X_n + t_n\epsilon_n, \quad (7)$$

$$t_n \sim \mathcal{U}(0, 1), \quad \epsilon_n \sim \mathcal{N}(0, I), \quad (8)$$

where  $E_{\text{vit}}$  denotes the vision encoder for understanding tokens, and  $E_{\text{vae}}$  is a *frozen* VAE encoder. We treat the concatenation for training-time

$$V_n = T_{\text{i}}(v_n; t_n, \epsilon_n) \triangleq [\tilde{X}_n^{(t_n)}, X_n, U_n] \quad (9)$$

as the image-token block for step  $n$ , where  $\epsilon_n$  is sampled noise. Within each image block, we order visual tokens as (noised VAE, clean VAE, ViT). We then build the per-step block

$$\mathbf{b}_n = (Z_n, V_n), \quad (10)$$

and the full training sequence

$$\mathbf{y} = (T_{\text{tx}}(x), \mathbf{b}_1, \dots, \mathbf{b}_N), \quad (11)$$

where special tokens delimit modalities via reserved textual tokens.

**Unified interleaved decoding.** Let  $ULM_\theta$  denote a unified multimodal decoder that (i) defines an autoregressive conditional distribution over text tokens given an interleaved prefix and (ii) implements a rectified-flow velocity predictor over VAE latents. SoT follows a *decide-then-ground* order: at step  $n$ , the model first generates the textual plan  $Z_n$  and then generates the rendered observation by rectified-flow sampling in the VAE latent space:

$$Z_n \sim ULM_\theta(\cdot \mid T_{\text{tx}}(x), \{Z_j\}_{j < n}, \{X_j, U_j\}_{j < n}), \quad (12)$$

$$\hat{X}_n \leftarrow \text{RF-Sample}(u_\theta; T_{\text{tx}}(x), \{Z_j\}_{j \leq n}, \{X_j, U_j\}_{j < n}), \quad (13)$$

$$\hat{v}_n = D_{\text{vae}}(\hat{X}_n), \quad (14)$$

where  $u_\theta$  is the rectified-flow velocity field predicted by  $ULM_\theta$  and queried during sampling, and  $D_{\text{vae}}$  is the *frozen* VAE decoder. After obtaining  $\hat{v}_n$ , we set  $X_n = \hat{X}_n$  and compute  $U_n = E_{\text{vit}}(\hat{v}_n)$  as deterministic conditioning tokens for subsequent steps (Appendix B). Importantly,  $X_n$  is produced via rectified-flow sampling in the continuous VAE latent space, and  $U_n$  is deterministically encoded from  $\hat{v}_n$ ; the model does not sample them as discrete codebook tokens.

### 3.2. SoT-26K Dataset

**Why SOT-26K?** Progressive assembly requires supervision beyond goal conditioning: the model must learn *how* structure evolves, step by step, with each textual decision grounded by a corresponding visual state. We therefore curate SOT-26K, a large-scale collection of *step-aligned* interleaved state–rationale traces. Two design principles make supervision more unambiguous. First, we enforce a fine-grained schedule where each step introduces a small batch of leaf parts that together form one semantic component, capped by a maximum batch size (e.g., 15–25 leaf parts per step for complex objects), yielding a uniquely defined structural delta  $\Delta P_n$ . Second, we constrain each rationale to a lightweight slot schema—(*new component*)

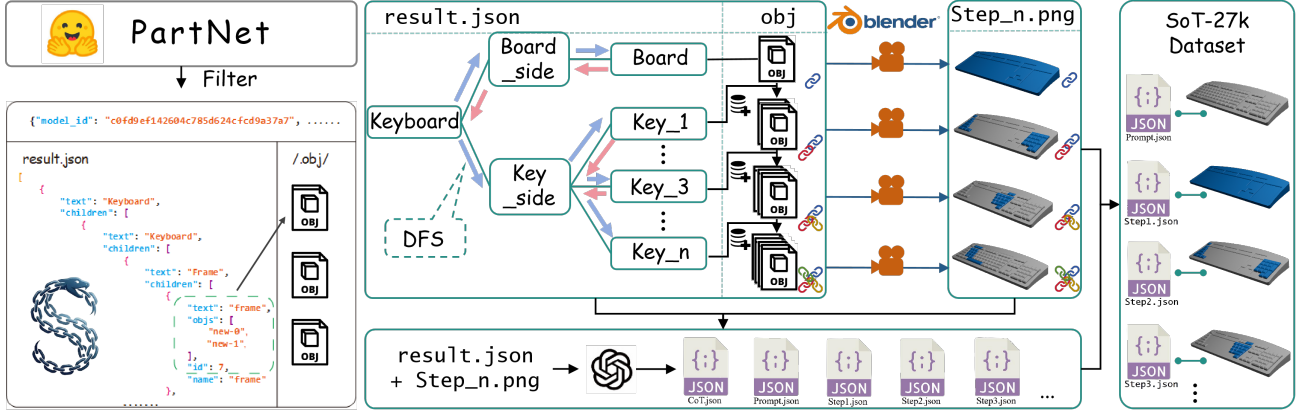


Figure 4. **The SoT-26K Construction Pipeline.** We transform PartNet assets into multimodal traces through four stages: (A) **Data Curation** to filter and validate raw hierarchies; (B) **Hierarchy Decomposition** to enforce fine-grained assembly schedules; (C) **Automated Rendering** to generate cumulative intermediate states in Blender; and (D) **Multimodal Annotation**, where GPT-4o synthesizes step-wise rationales and goal prompts grounded in the visual evidence.

+ (attachment relation) + (anchor on existing structure)—to promote semantic consistency and discourage free-form hallucinations.

**Dataset overview.** SOT-26K contains **25,929** object traces (denoted as 26K for brevity) across **24** diverse object categories, each paired with a single goal prompt  $x$  describing the target object. Although derived from part-based 3D CAD assets dataset PartNet (Mo et al., 2019), SOT-26K is packaged as a vision–language dataset: all supervision is delivered via *2D renderings* produced by a fixed Blender protocol under a canonical front camera. Future work will extend to multi-view settings with left/right/back cameras.

**Interleaved trace definition.** Each instance is represented as a progressive assembly trace

$$\mathcal{T} = [x, (z_1, v_1), (z_2, v_2), \dots, (z_N, v_N)], \quad (15)$$

where  $x$  is the goal prompt,  $v_n$  is the rendered image of the cumulative assembly at step  $n$ , and  $z_n$  is a concise rationale grounded in the transition from step  $n-1$  to  $n$ . Let  $P_{\leq n}$  denote the cumulative set of assembled parts at step  $n$  (with  $P_{\leq 0} = \emptyset$ ). Under our fine-grained assembly schedule, the newly added parts at step  $n$  are uniquely defined as

$$\Delta P_n = P_{\leq n} \setminus P_{\leq n-1}. \quad (16)$$

We generate  $z_n$  to explicitly describe  $\Delta P_n$  and its attachment to an existing anchor in  $P_{\leq n-1}$ , while  $v_n$  provides visual evidence of the updated structure.

**Construction pipeline.** We construct SOT-26K from PartNet-style assets through four stages: (A) **Data curation and loading** preprocesses the raw PartNet dataset by removing duplicates and organizing samples by category,

then loads and validates JSON hierarchies. (B) **Hierarchy decomposition** parses the part tree and produces an ordered leaf-part schedule  $\{P_{\leq n}\}_{n=1}^N$ , enforcing a fine-grained assembly schedule (Eq. 16). (C) **Automated rendering** generates the cumulative intermediate states  $\{v_n\}$  in headless Blender under a canonical front camera. (D) **Multimodal annotation** uses an MLLM (GPT-4o) to generate the goal prompt  $x$  from the final rendering and to produce step rationales  $\{z_n\}$  grounded in  $\Delta P_n$  and conditioned on rendered visual evidence. Full implementation details, file formats, and prompt templates are provided in Appendix A.2.

### 3.3. Model and Training

**Instantiation.** We instantiate ULM $_{\theta}$  in Sec. 3.1 with Bagel-7B (MoT variant), a unified multimodal autoregressive Transformer (Deng et al., 2025). The MoT architecture employs hard routing where VAE generation tokens are processed by a dedicated generation expert, while text tokens and ViT understanding tokens are handled by the understanding expert. Given the serialized interleaved stream  $y$  (Eq. 11), Bagel performs early-fusion modeling by attending jointly over textual tokens (plans and delimiters) and interleaved image blocks composed of continuous VAE latent tokens (for generation) and ViT understanding tokens (for perception). Here, ‘token’ refers to an element in the multimodal sequence: text tokens are discrete, while visual-latent tokens are continuous VAE latents projected into the model’s embedding space. This design enables tight coupling between structural planning and visual grounding.

**Training and inference.** We train with teacher forcing on the serialized interleaved stream  $y$  (Eq. 11). Text tokens are optimized with standard next-token cross-entropy, while visual segments are optimized by regressing the tar-

**Table 1. Quantitative Results on T2S-CompBench.** We compare SoT against 2D generative baselines and 3D synthesis methods. Note that **Meshy 6** is included as a *commercial reference* for strong appearance quality. **SoT** demonstrates superior structural compliance significantly on Numeracy (CN) and Topology (VT) in the projected views. The **best** and **second-best** scores are highlighted. The last column reports the average **Human Evaluation** score (1–5 scale) across Visual Quality, Structural Correctness and Construction Logic. RA/TS require visual traces while some baselines only provide final assets (–).

Method	T2S-Structure					T2S-Process		Human (1–5)†	Latency / s
	CN↑	SF↑	AF↑	CP↑	VT↑	RA↑	TS↑		
<i>2D Generative Baselines</i>									
Bagel-7B	64.26	71.57	58.34	62.14	65.42	–	–	3.12	51.95
Bagel-7B-CoT†	75.88	74.23	72.16	68.92	71.38	45.49	32.71	3.65	103.46
<i>Rendered 3D baselines‡</i>									
Shap-E (Jun & Nichol, 2023)	42.15	75.38	25.23	21.11	28.59	–	–	1.85	9.92
LGM (Tang et al., 2025)	68.62	80.15	55.40	72.30	76.50	–	–	3.25	6.48
L3GO (Yamada et al., 2025)	76.20	65.80	68.45	60.10	72.90	–	–	3.05	921.27°
Meshy 6*	82.74	95.43	75.27	85.60	78.25	–	–	3.91	74.81
<b>Bagel-7B-SoT</b>	<b>88.44</b>	83.62	<b>81.51</b>	<b>86.25</b>	<b>84.76</b>	<b>79.19</b>	<b>91.30</b>	<b>4.08</b>	43.14 (per step) / 257.75 (total)

† For *Bagel-7B-CoT*, we generate the full textual CoT first, then sample corresponding images.

‡ We render 3D baselines’ outputs with the same canonical camera protocol.

° L3GO relies on iterative trial-and-error loops within the Blender environment.

\* Meshy 6 is a closed-source commercial service evaluated via the Meshy 6 API (no-texture mode). <https://www.meshy.ai/blog/meshy-6-launch>.

get visual latents produced by the *frozen* pretrained image tokenizer/VAE.

We fine-tune the Bagel-7B Transformer backbone jointly with the ViT encoder, while keeping the pretrained VAE tokenizer (encoder/decoder) frozen. Optimization follows Table 4 (AdamW, cosine LR with warmup, gradient clipping, EMA, token-budgeted batching). At inference time, the model decodes the interleaved stream in the *decide-then-ground* order (Eqs. 12–14) until the final visual segment  $V_N$  is produced; decoding  $V_N$  through the fixed VAE yields the final rendered output. Additional training and decoding details are provided in Appendix B.

### 3.4. Evaluation Benchmark: T2S-CompBench

Appearance-centric metrics (Hessel et al., 2021; Huang et al., 2025) do not assess whether an object is constructed through a step-faithful and stable trace. We therefore introduce **T2S-CompBench (Text-to-Shape)**, a process-aware benchmark with two axes: **T2S-Structure** evaluates whether the final rendering  $v_N$  satisfies the goal prompt  $x$ , and **T2S-Process** evaluates whether the intermediate trace  $\{v_1, \dots, v_N\}$  is stable and step-faithful. T2S-Structure reports five forced-choice metrics: **CN** (Component Integrity and Numeracy), **SF** (Shape Fidelity), **AF** (Attribute Fidelity), **CP** (Connectivity Plausibility), and **VT** (Visual Topology). T2S-Process reports two trace metrics: **TS** (Trace Stability) and **RA** (Step-wise Rationale Alignment). Details and formulas are shown in Appendix E.

We adopt a hybrid evaluation protocol tailored to our rendered domain: GPT-4o (Hurst et al., 2024) (API) provides closed-form forced-choice decisions for semantic/relational

metrics ( $\{\text{CN, SF, AF, CP, VT, RA}\}$ ), while SAM 3 (Carion et al., 2025) union foreground masks are used to compute TS. Unless otherwise noted, all metrics are computed on the canonical **front** view. To validate robustness against potential VLM-as-a-judge bias, we re-audit a stratified subset with an alternative open-weight VLM (Qwen2-VL-7B-Instruct) and quantify cross-judge consistency in Appendix G.

### 3.5. Human Evaluation

We conduct a human perceptual study on the final synthesized results to complement automated metrics. Each example is rated on a **5-point Likert scale** along three aspects: (1) **Visual Quality** (fidelity and details), (2) **Structural Correctness** (topology and completeness), and (3) **Construction Logic** (whether the final object exhibits a physically plausible assembly structure). We report the mean score averaged over the three aspects. The full study protocol (sampling, blinding/randomization, aggregation, confidence intervals, and agreement) is provided in Appendix F.

## 4. Experiments

**Data.** We use SOT-26K (Sec. 3.2), consisting of 25,929 3D models across 24 object categories, each containing interleaved text–image assembly traces. We split the annotated data into 69.9%/10.1%/20.0% for train/val/test following the original PartNet split (Mo et al., 2019), resulting in 18,141 training samples, 2,619 validation samples, and 5,169 test samples. Unless otherwise specified, we train and evaluate using the canonical **front** view, and truncate each serialized sequence to at most 50K tokens under token-budgeted batching with a soft target of 40K tokens per batch.

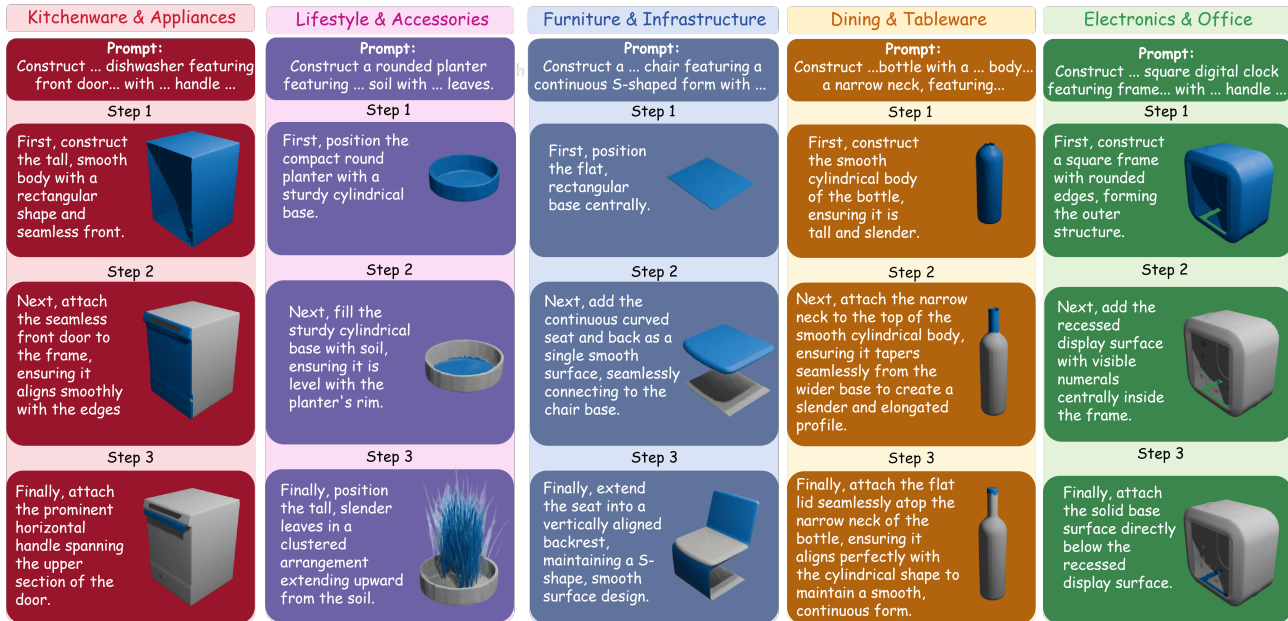


Figure 5. Visualization of Visual Chain-of-Thought Traces. SoT generates objects by progressively decomposing the goal into sequential sub-tasks. At each step, the model generates a structural rationale followed by the corresponding grounded visual state.

**Model.** We fully fine-tune BAGEL-7B (MoT variant) (Deng et al., 2025) end-to-end for interleaved text and visual-latent generation. Specifically, we perform full-parameter fine-tuning of the language model and vision transformer backbone modules, while keeping the VAE encoder/decoder frozen. All experiments are conducted on 32×NVIDIA H100 (80GB) GPUs.

**Optimization.** We train for 2,000 steps with AdamW ( $\beta_1=0.9$ ,  $\beta_2=0.95$ ,  $\epsilon=10^{-8}$ ), a cosine learning-rate schedule with 50 warmup steps, peak learning rate  $2 \times 10^{-5}$ , and minimum learning rate  $10^{-6}$ . We clip gradients to a global norm of 1.0 and use EMA with decay 0.9999. We cap the token budget by setting the expected number of tokens per step to 40K and the maximum to 50K (with max 50K per sample). Additional hyperparameters are deferred to Appendix D.

#### 4.1. Results

**Main results on T2S-CompBench.** Table 1 compares SoT with (i) direct generation and text-only CoT 2D generation on the same Bagel-7B backbone, and (ii) representative 3D synthesis / tool-driven systems (Shap-E, LGM, Meshy 6) whose outputs are evaluated via our canonical rendering protocol. SoT achieves the best performance on the majority of **T2S-Structure** metrics, demonstrating superior compliance in part counting (CN), attributes (AF), and spatial topology (VT). Compared to text-only **CoT** sampling, SoT yields especially large gains on assembly-critical constraints (e.g., attachment and spatial relations), while maintaining high

fidelity on part-bound attributes.

SoT additionally enables **T2S-Process** evaluation by generating explicit intermediate states. Interleaving rendered states substantially stabilizes the generation trajectory: TS improves from 32.71 to 91.30, and step-wise rationale alignment reaches 79.19. These results suggest that supervising decide-then-ground traces helps the model maintain a consistent visual working memory over multi-step assembly, reducing drift and uncontrolled re-drawing across steps.

**Rendered-view structural projection comparison.** Instead of treating native 3D generation methods as direct baselines, we include them to benchmark the difficulty of compositional constraints in the 3D domain. We render their outputs into canonical views to evaluate whether their underlying geometry projects to coherent structures that respect the assembly logic. While we acknowledge a domain gap in rendering styles, our primary objective is to verify structural integrity. This comparison serves as a proxy to verify if current 3D models can inherently handle fine-grained instruction following, independent of their generative modality.

Shap-E and LGM (Jun & Nichol, 2023; Tang et al., 2025) attain reasonable Shape Fidelity (SF), they struggle with fine-grained binding and topology (AF/CP). Meshy 6 achieves strong global connectivity (SF/CP) yet falls short on strict compositional constraints, specifically Numeracy (CN) and Attributes (AF) due to hallucinations and detail omission.

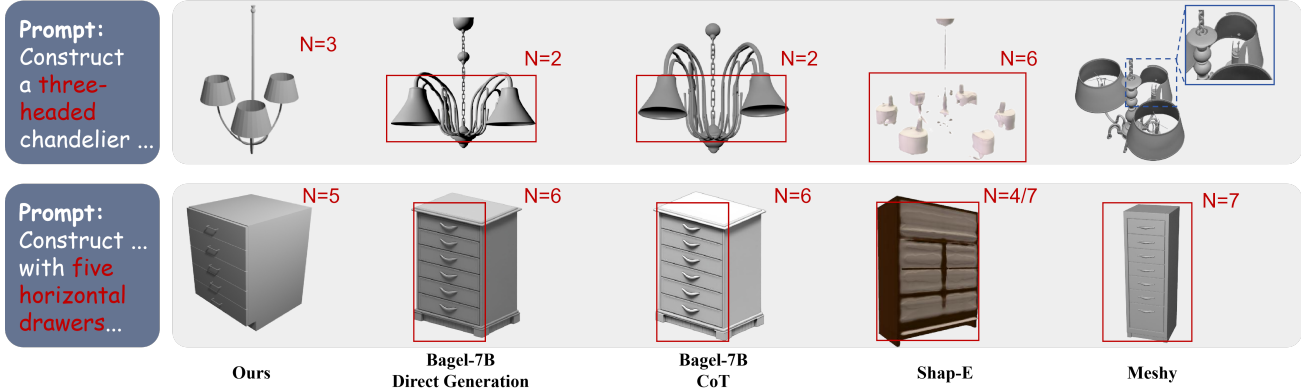


Figure 6. **Comparison on Numeracy and Topology.** SoT more consistently generates “three heads” and “five drawers” with valid topology, whereas baselines fail numeracy or suffer from structural collapse.

**Visualization.** Figure 5 visualizes the complete inference traces. Unlike black-box generation, SoT explicitly decomposes high-level goals into sequential visual sub-tasks, alternating between textual rationales and grounded visual states. For instance, in the **S-shaped chair** example (3rd column), the model maintains global geometric consistency, making the backrest connects seamlessly to the base rather than floating. This suggests that intermediate renderings serve as a **visual working memory**, facilitating the model to self-correct and verify structural integrity step-by-step.

**Qualitative Analysis: Numeracy and Topology.** Figure 6 highlights SoT’s higher compositional compliance than the compared baselines on T2S-CompBench **First**, regarding numeracy, 2D baselines exhibit characteristic semantic drift, frequently violating discrete count constraints, while Meshy—despite clean geometry—still often over/under-produces repeated components under compositional requirements. **Second, regarding topology and detail fidelity**, Shap-E can collapse into structurally implausible artifacts, and Meshy may smooth out or drop secondary structures even when the overall silhouette looks correct. In contrast, SoT treats intermediate visual states as explicit grounding, preserving previously assembled structures and thus prioritizing numeracy and topology fidelity.

## 4.2. Ablation Study

Table 2 analyzes the impact of mechanism and data choices. Regarding mechanism, removing interleaved visual states (*No Visual Thoughts*) degrades structural logic (CP drops from 86.25 to 68.92), while masking visual history (*w/o Visual History*) notably impacts stability (TS decreases to 42.83), suggesting the role of visual working memory. In terms of data, replacing the structured schema with free-form text (*Free-form Rationale*) reduces Rationale Alignment (RA drops to 55.47) while maintaining similar structural scores, indicating that the schema specifically aids in

Table 2. **Ablation Study.** We validate key design choices across mechanism, data, and optimization. **Full Model** is Bagel-7B (SoT). *No Visual Thoughts* removes interleaved image generation. *w/o Visual History* masks attention to prior visual tokens. *Free-form Rationale* removes the structured text schema.

Variant	Structure				Process	
	CN ↑	AF ↑	CP ↑	VT ↑	RA ↑	TS ↑
<b>SoT (Full Model)</b>	<b>88.44</b>	<b>81.51</b>	<b>86.25</b>	<b>84.76</b>	<b>79.19</b>	<b>91.30</b>
<i>A. Mechanism</i>						
No Visual Thoughts	75.88	72.16	68.92	71.38	45.49	32.71
w/o Visual History	84.32	78.17	65.44	67.51	71.16	42.83
<i>B. Data Construction</i>						
Free-form Rationale	86.59	79.80	83.13	82.94	55.47	88.25

aligning semantic plans with visual updates.

## 5. Conclusion

We introduced **Shape-of-Thought (SoT)**, a framework reframing shape generation as progressive assembly via interleaved text-image traces. To facilitate this paradigm, we curated the **SoT-26K** dataset and established **T2S-CompBench** for rigorous structural evaluation. This approach enables a single multimodal model to perform stepwise generation in image space without external 3D engines. Our results validate that intermediate visual states serve as an effective reasoning substrate for structural composition under rendered supervision.

**Discussion.** Building on SoT, future research may consider several important directions:

1. **From SoT renders to textured 3D assets.** A natural extension is to generate renders using SoT and lift them to 3D assets via a SAM3D-style mask-to-3D pipeline (Team et al., 2025). We provide a prelimi-



nary proof-of-concept for this extension in Appendix I, demonstrating that SoT’s structural renderings can be lifted to 3D meshes using off-the-shelf tools.

2. **Efficient training for multi-view.** Develop compute-aware strategies to unlock multi-view supervision, which is currently constrained by the prohibitive computational costs of dense visual traces (already saturating  $32 \times H100$  GPUs). We provide a detailed limitation and mitigation directions in Appendix H.
3. **Physical interpretability beyond transparent traces.** Although SoT exposes intermediate rationales and states, the learned procedure is not yet interpretable in terms of physical constraints, limiting faithful “assembly” understanding.

## Impact Statement

**Broader Impact.** This paper introduces Shape-of-Thought (SoT), a framework that reframes structural object generation as a progressive, interpretable visual reasoning process. By shifting from opaque, black-box synthesis to a transparent, step-by-step assembly paradigm, our work contributes to the development of more controllable and explainable AI systems.

**Interpretability and User Control.** A key societal benefit of SoT is the enhancement of transparency in generative AI. Traditional text-to-3D models often function as “black boxes,” making it difficult for users to understand why a specific geometry was generated or to correct errors. SoT’s visual chain-of-thought allows users to inspect the intermediate rationale and visual states. This interpretability is crucial for professional applications where verifying the structural logic is as important as the final appearance.

**Ethical Considerations and Risks.** We acknowledge potential risks associated with generative models. Like all models trained on large-scale datasets, SoT may inherit biases present in the training data (Mo et al., 2019), potentially reflecting cultural stereotypes in object design. Furthermore, while the focus of this work is on inanimate objects, the technology could theoretically be adapted to generate harmful content. We have focused our dataset on safe, common object categories, but future deployment should include rigorous safety filters and content moderation mechanisms.

## References

Asim, M., Wewer, C., Wimmer, T., Schiele, B., and Lenssen, J. E. Met3r: Measuring multi-view consistency in generated images. In *Proceedings of the Computer Vision and Pattern Recognition Conference*, pp. 6034–6044, 2025.

Carion, N., Gustafson, L., Hu, Y.-T., Debnath, S., Hu, R., Suris, D., Ryali, C., Alwala, K. V., Khedr, H., Huang, A., Lei, J., Ma, T., Guo, B., Kalla, A., Marks, M., Greer, J., Wang, M., Sun, P., Rädle, R., Afouras, T., Mavroudi, E., Xu, K., Wu, T.-H., Zhou, Y., Momeni, L., Hazra, R., Ding, S., Vaze, S., Porcher, F., Li, F., Li, S., Kamath, A., Cheng, H. K., Dollár, P., Ravi, N., Saenko, K., Zhang, P., and Feichtenhofer, C. Sam 3: Segment anything with concepts, 2025. URL <https://arxiv.org/abs/2511.16719>.

Cha, J. and Kim, J. Cot-pose: Chain-of-thought reasoning for 3d pose generation from abstract prompts. *arXiv preprint arXiv:2508.07540*, 2025.

Chen, Z., Zhou, Q., Shen, Y., Hong, Y., Sun, Z., Gutfreund, D., and Gan, C. Visual chain-of-thought prompting for knowledge-based visual reasoning. *Proceedings of the AAAI Conference on Artificial Intelligence*, 38(2):1254–1262, Mar. 2024. doi: 10.1609/aaai.v38i2.27888. URL <https://ojs.aaai.org/index.php/AAAI/article/view/27888>.

Cheng, Z., Chen, Q., Xu, X., WANG, J., Wang, W., Fei, H., Wang, Y., Wang, A. J., Chen, Z., Che, W., and Qin, L. Visual thoughts: A unified perspective of understanding multimodal chain-of-thought. In *The Thirty-ninth Annual Conference on Neural Information Processing Systems*, 2025. URL <https://openreview.net/forum?id=xPcKmKSEis>.

Deng, C., Zhu, D., Li, K., Gou, C., Li, F., Wang, Z., Zhong, S., Yu, W., Nie, X., Song, Z., et al. Emerging properties in unified multimodal pretraining. *arXiv preprint arXiv:2505.14683*, 2025.

Dong, Y., Liu, Z., Sun, H.-L., Yang, J., Hu, W., Rao, Y., and Liu, Z. Insight-v: Exploring long-chain visual reasoning with multimodal large language models. In *Proceedings of the IEEE/CVF Conference on Computer Vision and Pattern Recognition (CVPR)*, pp. 9062–9072, June 2025.

Dosovitskiy, A., Beyer, L., Kolesnikov, A., Weissenborn, D., Zhai, X., Unterthiner, T., Dehghani, M., Minderer, M., Heigold, G., Gelly, S., Uszkoreit, J., and Houshy, N. An image is worth 16x16 words: Transformers for image recognition at scale. In *International Conference on Learning Representations*, 2021. URL <https://openreview.net/forum?id=YicbFdNTTy>.

Gu, J., Hao, Y., Wang, H. W., Li, L., Shieh, M. Q., Choi, Y., Krishna, R., and Cheng, Y. Thinkmorph: Emergent properties in multimodal interleaved chain-of-thought reasoning, 2025. URL <https://arxiv.org/abs/2510.27492>.

- He, Y., Bai, Y., Lin, M., Zhao, W., Hu, Y., Sheng, J., Yi, R., Li, J., and Liu, Y.-J. T<sup>3</sup> bench: Benchmarking current progress in text-to-3d generation. *arXiv preprint arXiv:2310.02977*, 2023.
- Hessel, J., Holtzman, A., Forbes, M., Le Bras, R., and Choi, Y. CLIPScore: A reference-free evaluation metric for image captioning. In Moens, M.-F., Huang, X., Specia, L., and Yih, S. W.-t. (eds.), *Proceedings of the 2021 Conference on Empirical Methods in Natural Language Processing*, pp. 7514–7528, Online and Punta Cana, Dominican Republic, November 2021. Association for Computational Linguistics. doi: 10.18653/v1/2021.emnlp-main.595. URL <https://aclanthology.org/2021.emnlp-main.595/>.
- Ho, J., Jain, A., and Abbeel, P. Denoising diffusion probabilistic models. *Advances in neural information processing systems*, 33:6840–6851, 2020.
- Hong, Y., Zhen, H., Chen, P., Zheng, S., Du, Y., Chen, Z., and Gan, C. 3d-llm: Injecting the 3d world into large language models. In *Advances in Neural Information Processing Systems (NeurIPS)*, 2023.
- Hong, Y., Zhang, K., Gu, J., Bi, S., Zhou, Y., Liu, D., Liu, F., Sunkavalli, K., Bui, T., and Tan, H. LRM: Large reconstruction model for single image to 3d. In *The Twelfth International Conference on Learning Representations*, 2024. URL <https://openreview.net/forum?id=s11U8vvsFF>.
- Huang, K., Duan, C., Sun, K., Xie, E., Li, Z., and Liu, X. T2i-compbench++: An enhanced and comprehensive benchmark for compositional text-to-image generation. *IEEE Transactions on Pattern Analysis and Machine Intelligence*, 47(5):3563–3579, 2025. doi: 10.1109/TPAMI.2025.3531907.
- Hurst, A., Lerer, A., Goucher, A. P., Perelman, A., Ramesh, A., Clark, A., Ostrow, A., Welihinda, A., Hayes, A., Radford, A., et al. Gpt-4o system card. *arXiv preprint arXiv:2410.21276*, 2024.
- Jun, H. and Nichol, A. Shap-e: Generating conditional 3d implicit functions. *arXiv preprint arXiv:2305.02463*, 2023.
- Kingma, D. P. and Welling, M. Auto-encoding variational bayes. *arXiv preprint arXiv:1312.6114*, 2013.
- Li, C., Wu, W., Zhang, H., Xia, Y., Mao, S., Dong, L., Vulić, I., and Wei, F. Imagine while reasoning in space: Multimodal visualization-of-thought. In *Forty-second International Conference on Machine Learning*, 2025. URL <https://openreview.net/forum?id=6vk6Xg24ZC>.
- Linghu, X., Huang, J., Zhu, Z., Jia, B., and Huang, S. Eliciting grounded chain-of-thought reasoning in 3d scenes. *arXiv preprint arXiv:2510.16714*, 2025.
- Lyu, Q., Havaldar, S., Stein, A., Zhang, L., Rao, D., Wong, E., Apidianaki, M., and Callison-Burch, C. Faithful chain-of-thought reasoning. In Park, J. C., Arase, Y., Hu, B., Lu, W., Wijaya, D., Purwarianti, A., and Krisnadhi, A. A. (eds.), *Proceedings of the 13th International Joint Conference on Natural Language Processing and the 3rd Conference of the Asia-Pacific Chapter of the Association for Computational Linguistics (Volume 1: Long Papers)*, pp. 305–329, Nusa Dua, Bali, November 2023. Association for Computational Linguistics. doi: 10.18653/v1/2023.ijcnlp-main.20. URL <https://aclanthology.org/2023.ijcnlp-main.20/>.
- Mo, K., Zhu, S., Chang, A. X., Yi, L., Tripathi, S., Guibas, L. J., and Su, H. Partnet: A large-scale benchmark for fine-grained and hierarchical part-level 3d object understanding. In *Proceedings of the IEEE/CVF Conference on Computer Vision and Pattern Recognition (CVPR)*, 2019.
- Ramesh, A., Dhariwal, P., Nichol, A., Chu, C., and Chen, M. Hierarchical text-conditional image generation with clip latents, 2022. URL <https://arxiv.org/abs/2204.06125>.
- Ren, T., Liu, S., Zeng, A., Lin, J., Li, K., Cao, H., Chen, J., Huang, X., Chen, Y., Yan, F., Zeng, Z., Zhang, H., Li, F., Yang, J., Li, H., Jiang, Q., and Zhang, L. Grounded sam: Assembling open-world models for diverse visual tasks, 2024. URL <https://arxiv.org/abs/2401.14159>.
- Rombach, R., Blattmann, A., Lorenz, D., Esser, P., and Ommer, B. High-resolution image synthesis with latent diffusion models. In *Proceedings of the IEEE/CVF conference on computer vision and pattern recognition*, pp. 10684–10695, 2022.
- Saharia, C., Chan, W., Saxena, S., Li, L., Whang, J., Denton, E. L., Ghasemipour, K., Gontijo Lopes, R., Karagol Ayan, B., Salimans, T., et al. Photorealistic text-to-image diffusion models with deep language understanding. *Advances in neural information processing systems*, 35: 36479–36494, 2022.
- Tang, J., Zheng, G., Yu, J., and Yang, S. Cotdet: Affordance knowledge prompting for task driven object detection. In *2023 IEEE/CVF International Conference on Computer Vision (ICCV)*, pp. 3045–3055, 2023. doi: 10.1109/ICCV51070.2023.00285.
- Tang, J., Chen, Z., Chen, X., Wang, T., Zeng, G., and Liu, Z. Lgm: Large multi-view gaussian model for high-resolution 3d content creation. In Leonardis, A., Ricci,

- E., Roth, S., Russakovsky, O., Sattler, T., and Varol, G. (eds.), *Computer Vision – ECCV 2024*, pp. 1–18, Cham, 2025. Springer Nature Switzerland. ISBN 978-3-031-73235-5.
- Team, C. Chameleon: Mixed-modal early-fusion foundation models, 2025. URL <https://arxiv.org/abs/2405.09818>.
- Team, S. D., Chen, X., Chu, F.-J., Gleize, P., Liang, K. J., Sax, A., Tang, H., Wang, W., Guo, M., Hardin, T., Li, X., Lin, A., Liu, J., Ma, Z., Sagar, A., Song, B., Wang, X., Yang, J., Zhang, B., Dollár, P., Gkioxari, G., Feiszli, M., and Malik, J. Sam 3d: 3dfy anything in images, 2025. URL <https://arxiv.org/abs/2511.16624>.
- Tian, S., Wang, R., Guo, H., Wu, P., Dong, Y., Wang, X., Yang, J., Zhang, H., Zhu, H., and Liu, Z. Ego-rl: Chain-of-tool-thought for ultra-long egocentric video reasoning, 2025. URL <https://arxiv.org/abs/2506.13654>.
- Wang, X. and Zhou, D. Chain-of-thought reasoning without prompting. In *The Thirty-eighth Annual Conference on Neural Information Processing Systems*, 2024. URL <https://openreview.net/forum?id=4Zt7S0B0Jp>.
- Wang, X., Wei, J., Schuurmans, D., Le, Q. V., Chi, E. H., Narang, S., Chowdhery, A., and Zhou, D. Self-consistency improves chain of thought reasoning in language models. In *The Eleventh International Conference on Learning Representations*, 2023. URL <https://openreview.net/forum?id=1PL1NIMMrw>.
- Wang, Y., Wu, S., Zhang, Y., Yan, S., Liu, Z., Luo, J., and Fei, H. Multimodal chain-of-thought reasoning: A comprehensive survey, 2025. URL <https://arxiv.org/abs/2503.12605>.
- Wei, J., Wang, X., Schuurmans, D., Bosma, M., Ichter, B., Xia, F., Chi, E. H., Le, Q. V., and Zhou, D. Chain of thought prompting elicits reasoning in large language models. In Oh, A. H., Agarwal, A., Belgrave, D., and Cho, K. (eds.), *Advances in Neural Information Processing Systems*, 2022. URL [https://openreview.net/forum?id=\\_VjQlMeSB\\_J](https://openreview.net/forum?id=_VjQlMeSB_J).
- Xie, X., Zou, C., Karumuri, M. G., Lenssen, J. E., and Pons-Moll, G. Mvgbench: Comprehensive benchmark for multi-view generation models. *arXiv preprint arXiv:2507.00006*, 2025.
- Yamada, Y., Chandu, K., Lin, B. Y., Hessel, J., Yildirim, I., and Choi, Y. L3GO: Language agents with chain-of-3D-thoughts for generating unconventional objects. In Dziri, N., Ren, S. X., and Diao, S. (eds.), *Proceedings of the 2025 Conference of the Nations of the Americas Chapter of the Association for Computational Linguistics: Human Language Technologies (System Demonstrations)*, pp. 456–469, Albuquerque, New Mexico, April 2025. Association for Computational Linguistics. ISBN 979-8-89176-191-9. doi: 10.18653/v1/2025.naacl-demo.37. URL <https://aclanthology.org/2025.naacl-demo.37/>.
- Yao, S., Zhao, J., Yu, D., Du, N., Shafran, I., Narasimhan, K., and Cao, Y. React: Synergizing reasoning and acting in language models. In *International Conference on Learning Representations (ICLR)*, 2023.
- Yu, L., Shi, B., Pasunuru, R., Muller, B., Golovneva, O., Wang, T., Babu, A., Tang, B., Karrer, B., Sheynin, S., et al. Scaling autoregressive multi-modal models: Pretraining and instruction tuning. *arXiv preprint arXiv:2309.02591*, 2023.
- Yuan, Z., Lan, H., Zou, Q., and Zhao, J. 3d-premise: Can large language models generate 3d shapes with sharp features and parametric control? *arXiv preprint arXiv:2401.06437*, 2024.
- Zhao, Q., Lu, Y., Kim, M. J., Fu, Z., Zhang, Z., Wu, Y., Li, Z., Ma, Q., Han, S., Finn, C., Handa, A., Lin, T.-Y., Wetzstein, G., Liu, M.-Y., and Xiang, D. Cot-vla: Visual chain-of-thought reasoning for vision-language-action models. In *2025 IEEE/CVF Conference on Computer Vision and Pattern Recognition (CVPR)*, pp. 1702–1713, 2025. doi: 10.1109/CVPR52734.2025.00166.
- Zhong, Z., Yan, H., Li, J., Liu, X., Gong, X., Zhang, T., Song, W., Chen, J., Zheng, X., Wang, H., and Li, H. Flowvla: Visual chain of thought-based motion reasoning for vision-language-action models, 2025. URL <https://arxiv.org/abs/2508.18269>.

## A. SoT-26K Details

### A.1. SoT-26K Statistics

Table 3 provides detailed statistics of SoT-26K, including category breakdown, assembly complexity, and step distributions. The dataset encompasses 25,929 3D models across 24 object categories, with each model converted into an assembly trace averaging 6.2 steps (range 2-12). Categories are organized by functional groups, with furniture dominating due to structural complexity. The step distribution reveals assembly complexity patterns: furniture objects average 7.5 steps, appliances 5.8 steps, and tools 4.2 steps.

Table 3. Detailed Statistics of SoT Dataset by Category

General Category	Sub Category	Count	Avg Steps	Percentage (%)
Furniture & Infrastructure	Table	8,227	7.6	31.7
	Chair	6,323	7.5	24.4
	StorageFurniture	2,269	8.1	8.8
	Door	230	2.9	0.9
	Bed	192	8.4	0.7
	<b>Subtotal</b>	<b>17,241</b>	<b>7.5</b>	<b>66.5</b>
Lifestyle & Accessories	Lamp	2,212	4.2	8.5
	Vase	1,086	1.8	4.2
	Hat	231	2.1	0.9
	Bag	126	2.6	0.5
	Scissors	68	4.8	0.3
	<b>Subtotal</b>	<b>3,723</b>	<b>3.4</b>	<b>14.4</b>
Electronics & Office	Display	930	3.6	3.6
	Clock	554	2.9	2.1
	Laptop	433	4.9	1.7
	Earphone	229	6.4	0.9
	Keyboard	156	7.0	0.6
	<b>Subtotal</b>	<b>2,302</b>	<b>4.1</b>	<b>8.9</b>
Kitchenware & Appliances	Faucet	648	4.4	2.5
	TrashCan	321	4.6	1.2
	Refrigerator	187	5.4	0.7
	Microwave	183	4.5	0.7
	Dishwasher	181	4.1	0.7
	<b>Subtotal</b>	<b>1,520</b>	<b>4.5</b>	<b>5.9</b>
Dining & Tableware	Bottle	436	2.8	1.7
	Knife	327	3.3	1.3
	Mug	192	2.3	0.7
	Bowl	188	1.5	0.7
	<b>Subtotal</b>	<b>1,143</b>	<b>2.6</b>	<b>4.4</b>
<b>Total</b>		<b>25,929</b>	<b>6.2</b>	<b>100.0</b>

**Step Distribution Analysis:** The dataset exhibits diverse assembly complexities across categories. Furniture objects show the highest step counts (7.5 average), reflecting their hierarchical part structures and multi-component assemblies. Dining objects have simpler assemblies (2.6 average), often consisting of basic geometric components. The step distribution follows a right-skewed pattern, with most objects (85%) requiring 4-9 assembly steps.

## A.2. SoT-26K Construction Details

**Overview.** This appendix provides additional details on the construction of SOT-26K, our large-scale dataset for progressive 3D object assembly. Starting from raw PartNet (Mo et al., 2019) CAD assets, we transform hierarchical 3D part structures into step-aligned multimodal traces suitable for training multimodal autoregressive models. The construction pipeline addresses several key challenges: (i) maintaining structural consistency across assembly steps, (ii) maintaining visual coherence in rendered intermediate states, (iii) generating semantically meaningful assembly prompts, and (iv) scaling the process to handle thousands of diverse objects.

Our dataset encompasses **25,929** 3D models spanning **24** diverse object categories, from furniture (tables, chairs, storage units) to appliances (refrigerators, microwaves) to everyday objects (bottles, scissors, bags). Each model is converted into an assembly trace with an average of 6.2 steps, resulting in **162,003** step-level annotations across all traces. Each trace consists of interleaved text-image pairs, where textual rationales describe incremental assembly decisions and images provide visual grounding of the resulting structural state.

The construction process is organized into four interdependent stages that progressively transform raw CAD data into training-ready multimodal sequences: **(A) Data curation and loading** helps ensure dataset quality and structural validity; **(B) Hierarchy decomposition** creates assembly schedules with controlled granularity; **(C) Automated rendering** produces consistent visual representations of intermediate states; **(D) Multimodal annotation** generates natural language descriptions aligned with visual changes.

Each stage incorporates quality control measures and handles edge cases specific to CAD data processing. The resulting dataset enables supervised learning of assembly logic, with each trace providing explicit step-by-step supervision for multimodal generation.

**Stage A: Data curation and loading.** **Input:** raw PartNet dataset with scattered sample folders containing `meta.json`, `result.json`, and `objs/` directories.

**Output:** validated part hierarchies organized by category with quality metrics.

The curation phase begins with systematic scanning of all sample directories to extract metadata from `meta.json` files. Each file contains essential identifiers: `model_id` (unique model identifier), `model_cat` (semantic category like "Chair" or "Table"), and `anno_id` (annotation version identifier). We perform deduplication by `model_id` to eliminate redundant instances that may arise from multiple annotation versions, to ensure each unique 3D model appears exactly once in our dataset. Samples are then organized by category to enable category-specific processing parameters in downstream stages.

For structural validation, we load each `result.json` file and traverse the part hierarchy using depth-first search. The hierarchy represents objects as trees where internal nodes denote part groupings and leaf nodes contain mesh references in the `objs/` directory. We extract all leaf nodes with valid mesh references, recording their semantic names, textual descriptions, and OBJ file paths. Validation checks include: (i) existence of referenced mesh files, (ii) non-empty part hierarchies, (iii) consistent naming conventions, and (iv) absence of degenerate geometries.

Quality control measures during this stage include logging of parsing failures, statistics on hierarchy depths and branching factors, and identification of samples requiring manual review. This preprocessing ensures that only structurally sound, properly annotated models proceed to assembly planning, with category organization enabling efficient batch processing and parameter tuning.

**Stage B: Hierarchy parsing and assembly scheduling.** **Input:** validated part hierarchies with leaf node collections.

**Output:** assembly sequences with controlled step granularity and semantic ordering.

Assembly scheduling transforms static part hierarchies into dynamic construction sequences that simulate realistic object assembly. For each object instance  $o$ , we extract the complete set of leaf parts  $\mathcal{L}(o) = \{p_1, \dots, p_N\}$  through depth-first traversal of the validated hierarchy. Each leaf part  $p_n$  encapsulates multiple attributes: semantic name (e.g., "seat", "backrest"), textual description, unique identifier, and associated mesh file path.

The core challenge is determining assembly order while maintaining structural plausibility and controlling sequence length. We implement a configurable assembly scheduler that balances between fine-grained (many small steps) and coarse-grained (fewer large steps) assembly. The scheduler uses category-specific parameters: furniture objects like tables and chairs use broader steps (up to 15 parts per step) to manage complexity, while precision objects like scissors and knives use finer steps

(maximum 5 parts per step) to preserve assembly precision.

Sequence ordering follows ergonomic and structural principles. Foundational parts such as bases, frames, and bodies are assembled first to establish stable foundations. Category-aware prioritization promotes object-specific assembly logic, such as assembling bottle bodies before necks or chair bases before seats. Symmetric parts like multiple legs or keyboard keys are batched together to maintain visual and structural coherence throughout the assembly process.

The resulting assembly schedule defines cumulative part sets:

$$P_{\leq n} = \{p_1, \dots, p_n\}, \quad n = 1, \dots, N. \quad (17)$$

This indicates that  $\Delta P_n = P_{\leq n} \setminus P_{\leq n-1}$  represents a meaningful incremental addition at each step.

Sequence statistics reveal the diversity of assembly complexity: tables average 9 steps (range 6-12), chairs average 7 steps (6-10), while simple objects like mugs average 3 steps (2-6). This variation is intended to help the model learn both simple and complex assembly patterns, with quality control verifying that no sequence exceeds maximum step limits or contains implausible orders.

**Stage C: Headless rendering of intermediate assembly states.** **Input:** assembly sequences  $\{P_{\leq n}\}$  with mesh file references.

**Output:** synchronized visual and metadata sequences for each assembly trace.

Rendering intermediate assembly states requires careful synchronization between 3D geometry and visual representation. For each step  $n$  in the assembly sequence, we compose the cumulative part set  $P_{\leq n}$  by importing all referenced OBJ meshes into a Blender scene. Meshes are scaled uniformly (3x factor) and positioned according to their original CAD coordinates, facilitating geometric consistency across assembly steps.

The rendering pipeline operates in headless mode for scalability, processing thousands of assembly states efficiently. We employ Blender’s Eevee renderer with optimized settings: 512x512 resolution, 8 samples for anti-aliasing, and transparent background to isolate object geometry. A canonical front camera ( $c_f$ ) provides consistent viewpoint across all samples, reducing viewpoint variance and focusing model attention on structural changes rather than camera motion.

Scene configuration includes standardized lighting (single key light at 45° elevation) and material assignment (uniform gray Principled BSDF shader for all parts). This controlled environment maintains visual consistency while highlighting structural relationships through shading and depth cues.

For each assembly step, we generate synchronized outputs. The visual state is captured in `step_{n}.png`, showing the rendered image of the cumulative assembly up to that step. Structural metadata is stored in `step_{n}.json`, containing the step index, cumulative part list, and change description. For the complete assembly, we provide `final_complete.png` and `final_complete.json` to represent the fully assembled object.

Quality assurance includes validation of mesh loading, detection of rendering artifacts, and verification that visual changes correspond to structural additions. Memory management through periodic cleanup prevents accumulation of orphaned data blocks during batch processing. The resulting visual sequences provide pixel-level grounding for each assembly decision, enabling the model to learn the visual consequences of structural choices.

**Stage D: Text annotation for goal and step rationales.** **Input:** rendered visual sequences and structural metadata for each assembly trace.

**Output:** natural language goal prompts and step-by-step rationales synchronized with visual states.

The annotation stage bridges visual assembly states with natural language descriptions, enabling multimodal training. We employ GPT-4o as the annotation engine, leveraging its vision-language capabilities to generate contextually appropriate descriptions, with a total API expenditure of \$1,092 for the full dataset.

**Goal prompt generation:** Each trace receives a single high-level instruction  $x$  describing the complete target object. The prompt combines the final rendered image  $v_N$  with the complete part list  $P_{\leq N}$ , instructing the model to generate imperative descriptions that capture both visual appearance and functional structure. Examples include "Build a sturdy wooden chair with four legs, cushioned seat, and curved backrest" or "Construct a modern refrigerator with double doors, stainless steel finish, and internal shelving." These instructions serve as global context for the entire assembly sequence. Prompt templates are shown in Appendix K.

**Step rationale generation:** For each incremental step  $n$ , we generate a precise rationale  $z_n$  explaining the structural change from  $v_{n-1}$  to  $v_n$ . The annotation follows a structured schema to improve consistency: *(action verb) + (new parts) + (attachment preposition) + (anchor location)*. Multimodal input includes the current step image  $v_n$ , previous step image  $v_{n-1}$  (for  $n > 1$ ), and the computed part difference  $\Delta P_n$ . The model is prompted to focus on essential structural relationships while avoiding redundant explanations.

Quality control measures include consistency validation through cross-checking that mentioned parts exist in  $\Delta P_n$ , semantic coherence by promoting rationales use appropriate assembly terminology, length control to maintain concise descriptions (typically 10-20 words per step), and category adaptation using domain-specific vocabulary (e.g., "blade" vs "seat").

The resulting annotations create a complete multimodal trace where each visual state is precisely described by its accompanying rationale, enabling the model to learn the mapping between structural decisions and their linguistic expression. This synchronization is crucial for training autoregressive models that can generate both coherent assembly sequences and appropriate explanatory text.

**Dataset packaging and directory structure. Output artifact:** self-contained multimodal traces with comprehensive metadata and quality assurance.

Each processed instance is converted into a structured Parquet record that encapsulates all multimodal components necessary for training. The Parquet format promotes efficient storage and loading of interleaved text-image sequences.

The dataset is released in Parquet format for efficient storage and loading, with the following structure:

```
SoT/
+-- Bottle/
|   +-- train/
|   |   +-- train-00000-of-00001.parquet
|   +-- val/
|   |   +-- val-00000-of-00001.parquet
|   +-- test/
|       +-- test-00000-of-00001.parquet
+-- Chair/
|   +-- train/
|   |   +-- train-00000-of-00001.parquet
|   +-- val/
|   |   +-- val-00000-of-00001.parquet
|   +-- test/
|       +-- test-00000-of-00001.parquet
+-- ... (other categories)
+-- Table/
|   +-- train/
|   |   +-- train-00000-of-00001.parquet
|   +-- val/
|   |   +-- val-00000-of-00001.parquet
|   +-- test/
|       +-- test-00000-of-00001.parquet
```

**Parquet file schema:** Each Parquet file contains the following fields for multimodal training:

- Prompt (string): The high-level goal instruction describing the target object
- Shape of Thought Reasoning Trace (string): Formatted assembly steps with image placeholders for progressive reasoning
- Final Assembly (string): Fixed-format final answer indicating assembly completion
- reasoning\_image\_N (struct): Intermediate assembly images with embedded bytes and relative paths

- `final_image` (struct): Complete assembled object image with embedded bytes and relative path

**Quality assurance:** The dataset maintains rigorous quality control through automated validation of mesh integrity, hierarchy consistency, rendering quality, annotation coherence, and multimodal synchronization. We employed 10 professional annotators to manually review critical cases and promote annotation quality. Images are embedded directly in Parquet files for efficient streaming during training.

This Parquet-based packaging enables efficient distributed training with embedded images, supports large-scale multimodal learning, and facilitates reproducible experiments across different object categories. The structured format with embedded visual data helps seamless integration with modern multimodal training pipelines.

## B. Training Details

**Vision tokenization.** For visual generation, we encode each rendered image into VAE (Kingma & Welling, 2013) latents using a pre-trained VAE and keep the VAE frozen during training. The latent features are further patch-embedded to match the Transformer hidden dimension.<sup>1</sup> We also obtain ViT tokens from a ViT encoder (Dosovitskiy et al., 2021) for visual understanding; both ViT and VAE tokens are equipped with 2D positional encoding, and rectified-flow time embeddings are added to the initial hidden states of noised VAE latent tokens.

**Generalized causal attention for interleaving.** Within each sample, tokens are partitioned into multiple consecutive modality splits (text / vision tokens), with the split order following the serialized token stream in Eq. 11. Inside each split, text uses causal attention; vision tokens use bidirectional attention within the split, while respecting the split-level causal ordering (a split cannot attend to future splits). Tokens in one split may attend to all tokens in preceding splits; inside each split, text uses causal attention while vision tokens use bidirectional attention. For each image segment, we maintain three sets of visual tokens: (i) noised VAE tokens used for rectified-flow training, (ii) clean VAE tokens used as conditioning for subsequent segments, and (iii) ViT tokens. Subsequent tokens may attend to the clean VAE and ViT tokens of preceding images, but not to the noised VAE tokens.

**Teacher forcing on interleaved streams.** Given a training instance  $(x, \mathcal{T})$  with  $\mathcal{T} = \{(z_n, v_n)\}_{n=1}^N$ , we serialize it into an interleaved token stream  $\mathbf{y} = (y_1, \dots, y_L)$  as in Eq. 11. We train  $\text{ULM}_\theta$  with teacher forcing: at text positions the model predicts the next token under the ground-truth prefix, while at noised-latent positions it predicts the rectified-flow velocity target under the same prefix.

**Token partitions.** Let  $\mathcal{V}_{\text{text}}$  denote the unified text vocabulary (including reserved delimiters for multimodal content). We define two disjoint index sets over positions in  $\mathbf{y}$ :

$$\mathcal{P}_{\text{text}} = \{t \mid y_t \in \mathcal{V}_{\text{text}}\}, \tag{18}$$

$$\mathcal{P}_{\text{mse}} = \{t \mid y_t \text{ corresponds to a noised VAE latent element } \tilde{X}_{n,m}^{(t_n)}\}. \tag{19}$$

Here  $\mathcal{P}_{\text{mse}}$  enumerates all positions corresponding to the *noised* VAE latent tokens inside the training-time image-token blocks  $V_n = [\tilde{X}_n^{(t_n)}, X_n, U_n]$ . We keep the VAE tokenizer components (VAE encoder/decoder) frozen, and fine-tune the Transformer backbone together with the ViT encoder. For notational simplicity, we denote all trainable parameters (Transformer + ViT) by  $\theta$ .

**Text objective: next-token cross-entropy.** We minimize the standard autoregressive cross-entropy over text-token positions:

$$\mathcal{L}_{\text{CE}}(\theta) = - \sum_{t \in \mathcal{P}_{\text{text}}} \log p_\theta(y_{t+1} \mid y_{\leq t}), \tag{20}$$

where we use the standard one-token shift and exclude the last position from  $\mathcal{P}_{\text{text}}$  when forming labels.

**Visual objective: MSE velocity regression.** For each rendered observation  $v_n$ , we obtain its clean VAE latents  $X_n = E_{\text{vae}}(v_n)$  and sample  $t_n \sim \mathcal{U}(0, 1)$  with  $\epsilon_n \sim \mathcal{N}(0, I)$ , constructing the noised latents along the linear path

$$X_n(t_n) = (1 - t_n)X_n + t_n\epsilon_n. \tag{21}$$

<sup>1</sup>Bagel uses a FLUX VAE with downsample ratio 8 and latent channel 16, followed by a  $2 \times 2$  patch embedding.



Under this linear path, the target *velocity* is constant:

$$u_n^* = \epsilon_n - X_n. \tag{22}$$

Let  $\hat{u}_t$  be the model prediction at a noised-latent position  $t \in \mathcal{P}_{\text{mse}}$  (produced by a regression head on top of  $\text{ULM}_\theta$ ). We minimize the mean-squared error over all noised latent tokens:

$$\mathcal{L}_{\text{MSE}}(\theta) = \sum_{t \in \mathcal{P}_{\text{mse}}} \|\hat{u}_t - u_t^*\|_2^2. \tag{23}$$

In practice, each  $t \in \mathcal{P}_{\text{mse}}$  corresponds to some latent element  $(n, m)$  in  $\tilde{X}_n^{(t_n)}$ , and  $u_t^*$  denotes the aligned element in  $u_n^*$ .

**Final training objective.** We optimize a weighted combination of the text cross-entropy loss and the visual velocity regression loss:

$$\min_{\theta} \mathbb{E}_{(x, \mathcal{T}) \sim \mathcal{D}} \left[ \lambda_{\text{CE}} \mathcal{L}_{\text{CE}}(\theta) + \lambda_{\text{MSE}} \mathcal{L}_{\text{MSE}}(\theta) \right], \tag{24}$$

where  $\lambda_{\text{CE}}$  and  $\lambda_{\text{MSE}}$  are scalar loss weights. We set  $\lambda_{\text{CE}} : \lambda_{\text{MSE}} = 1 : 1$  in our experiments to emphasize both text planning quality and visual generation accuracy. In our implementation,  $\lambda_{\text{CE}}$  corresponds to `ce_weight` and  $\lambda_{\text{MSE}}$  corresponds to `mse_weight`.

**Optimization and decoding.** We train for 2,000 steps with AdamW optimizer ( $\beta_1 = 0.9$ ,  $\beta_2 = 0.95$ ,  $\epsilon = 10^{-8}$ , weight decay 0), using a cosine learning-rate schedule with 50 warmup steps (peak LR  $2 \times 10^{-5}$ , min LR  $10^{-6}$ ). We clip gradients to a global norm of 1.0 and use EMA with decay 0.9999. Training uses token-budgeted batching with an expected 40K tokens per step and a hard cap of 50K tokens. Each serialized sample is truncated to at most 50K tokens. During packing, if a truncated sample cannot fit into the remaining token budget of the current step, we defer it into an overflow buffer and prioritize sampling from this buffer when the step budget is under 20K tokens. All training is conducted in bfloat16 using FSDP (HYBRID\_SHARD; CPU offload enabled).

At inference time, we use classifier-free guidance with text scale 4.0, image scale 2.0, and guidance interval  $[0.0, 1.0]$ . To support CFG, we apply the same modality-dropout to the conditioning prefix during training, dropping text, VAE, and ViT conditioning tokens with probabilities 0.1, 0.3, and 0.3, respectively, to construct unconditional prefixes. We compute conditional and unconditional predictions and apply CFG as  $\hat{u} = u_{\text{uncond}} + s_{\text{img}}(u_{\text{cond}} - u_{\text{uncond}})$  for RF velocity, and similarly for text logits with scale  $s_{\text{text}}$ .

We alternate between (i) sampling text plans autoregressively with temperature 0.3 (Eq. 12) and (ii) sampling VAE latents with rectified flow using 50 timesteps and timestep shift 1.0 (Eq. 13), followed by decoding through the frozen VAE decoder (Eq. 14). After obtaining  $\hat{v}_n$ , we set  $X_n = \hat{X}_n$  and compute  $U_n = \mathbb{E}_{\text{vit}}(\hat{v}_n)$  as deterministic conditioning tokens for subsequent steps.

### C. Inference Termination Mechanism

The Shape-of-Thought (SoT) framework employs a carefully designed termination mechanism to determine when the progressive assembly process should conclude. This mechanism ensures that the model generates an appropriate number of assembly steps and produces a coherent final output without over-generation or premature termination.

Our termination mechanism consists of two complementary signals:

**Structural Termination Marker (Training).** During training, we use a structured termination marker to teach the model when assembly is complete. Each training example contains a `Final Assembly` field formatted as `<assembly>Final Assembly: FINISH</assembly>`. This marker serves as a clear signal that the progressive assembly process has reached its conclusion. The model learns to predict this token sequence at the appropriate moment, effectively learning when enough structural components have been assembled to satisfy the goal prompt.

The training data constructs interleaved sequences where each reasoning step text is wrapped in `<thought>` and `</thought>` tokens, each image is bounded by `<image_start>` and `<image_end>` tokens, and the final assembly confirmation is wrapped in `<assembly>` and `</assembly>` tokens.

Table 4. Training hyperparameters (aligned with the main-text Optimization paragraph).

Item	Value
Backbone	Bagel-7B (MoT; Qwen2MoTDecoderLayer)
Training steps	2,000
Optimizer	AdamW ( $\beta_1=0.9$ , $\beta_2=0.95$ , $\epsilon=10^{-8}$ )
Weight decay	0
LR schedule	cosine
Warmup steps	50
Peak LR / min LR	$2 \times 10^{-5}$ / $10^{-6}$
Grad clip	1.0 (global norm)
EMA decay	0.9999
Loss weights (CE / MSE)	1 / 1
Token budget (expected / max)	40K / 50K tokens per step
Max tokens / sample	50K (truncate; overflow-buffer packing for budget overflow)
Max latent size	64
Precision	bfloat16
Sharding	FSDP, HYBRID_SHARD (32 shards; CPU offload enabled)
Conditioning dropout (text / VAE / ViT)	0.1 / 0.3 / 0.3
Frozen modules	VAE (encoder/decoder/tokenizer)
Trainable modules	Transformer backbone + ViT encoder
Seeds (data / global)	42 / 4,396
Infrastructure	32× NVIDIA H100 80GB; Python 3.10.19; Linux (glibc 2.35)

**Token-Level Termination (Inference).** At inference time, we employ a token-level termination detection mechanism implemented in the `generate_text` function. The model uses the end-of-sequence token (`<|im_end|>`) as the primary termination signal. When this token is generated, the termination mechanism performs an additional lookahead step: if the next token is `<|vision_start|>`, the generation continues to produce the corresponding image; otherwise, the generation loop terminates. A maximum token limit (`max_length`) provides a hard cap to prevent infinite generation loops.

This lookahead mechanism is essential because the end-of-sequence token may appear in two distinct contexts: (1) **True Termination**: the model has completed assembly and signals the end of generation; (2) **Image Block Transition**: the model signals the end of the current text block and expects to generate the next image.

The termination mechanism enables SoT to automatically determine the appropriate number of assembly steps for each object, adapting to the inherent complexity of the target structure without requiring explicit step-count specification from the user.

## D. Experimental Details

### D.1. Hyperparameters and infrastructure.

We fine-tune Bagel-7B end-to-end with AdamW ( $\beta_1=0.9$ ,  $\beta_2=0.95$ ,  $\epsilon=10^{-8}$ ) for 2,000 optimization steps. We use a cosine learning-rate schedule with 50 warmup steps (peak LR  $2 \times 10^{-5}$ , min LR  $10^{-6}$ ), global gradient clipping at 1.0, and exponential moving average (EMA) with decay 0.9999. Training uses bfloat16 with FSDP under a HYBRID\_SHARD strategy (32 shards) and CPU offloading enabled. We adopt token-budgeted batching with an expected 40K tokens per step and a hard cap of 50K tokens, truncating each serialized sample to at most 50K tokens (and skipping over-limit samples with an overflow buffer). We freeze the VAE while fine-tuning the Transformer and the ViT modules; dropout probabilities are 0.1 for text conditioning and 0.3 for VAE/ViT conditioning. All experiments are run with fixed data/global seeds (42 / 4,396) on 32× NVIDIA H100 (80GB) GPUs.

### D.2. Training Metrics Visualization

Figure 7 presents the evolution of key training metrics over the course of 2,000 optimization steps. The visualization provides insights into the stability and convergence behavior of our model:

- **Data Throughput and Tokens:** Subfigure (a) illustrates the *Total Samples per Step*, which, after an initial startup

### Training Metrics Over Steps

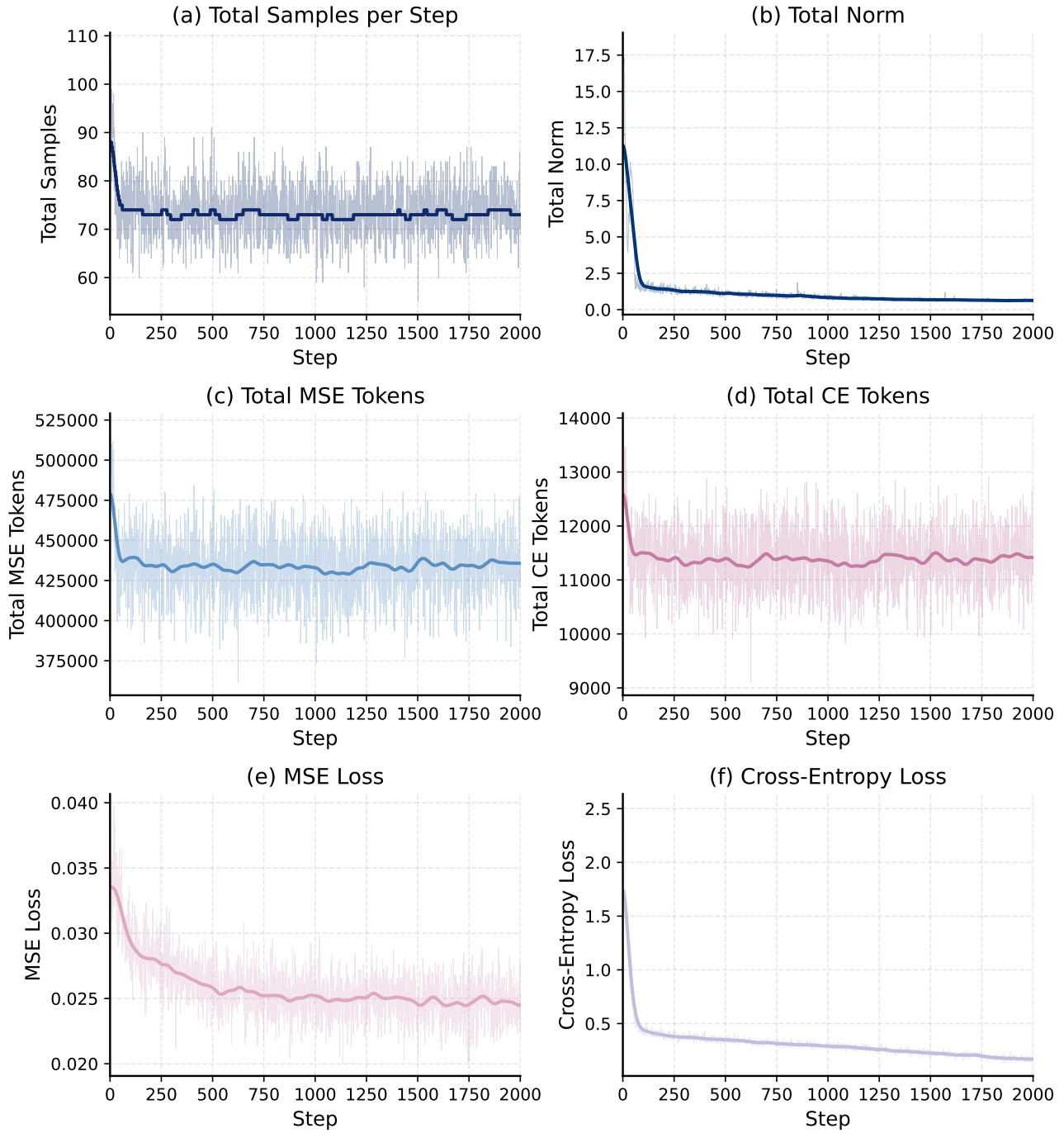


Figure 7. **Training Metrics Over Steps.** Complete training visualization including: (a) Total samples per step, (b) Total norm, (c-d) MSE and CE token counts, (e-f) Loss curves.

phase, stabilizes at approximately 73 samples per step. Similarly, subfigures (c) and (d) show the *Total MSE Tokens* and *Total CE Tokens* respectively. These metrics remain consistent throughout the training process (averaging roughly 435,000 MSE tokens and 11,400 CE tokens per step), indicating a stable data pipeline and consistent batch composition.

- **Optimization Stability:** Subfigure (b) displays the *Total Norm* of the gradients. We observe a sharp initial decrease from a peak of over 12.5 to below 2.5 within the first 100 steps, followed by a gradual, smooth decline. This behavior suggests that the optimization process is well-conditioned and free from significant gradient explosions, leading to stable parameter updates.
- **Loss Convergence:** The primary objectives, *MSE Loss* (e) and *Cross-Entropy (CE) Loss* (f), both demonstrate clear downward trajectories. The MSE loss steadily decreases from 0.035 and begins to plateau around 0.025. The CE loss exhibits a more rapid initial descent from 2.5, continuing a sustained decline towards 0.2 by the end of 2,000 steps. The lack of significant spikes in either loss curve confirms that the learning rate schedule and optimization strategy are effective for joint regression and classification tasks.

Overall, these metrics confirm a healthy training regime with consistent token throughput and steady convergence across multiple objective functions.

## E. T2S-CompBench: Implementation Details

### E.1. Pilot Human Audit for Protocol Selection

To choose reliable evaluators in our rendered domain, we conducted a pilot human audit on fine-grained component recognition. We selected 24 component sub-classes and sampled 10 rendered images per class. For each image, we derive per-component text prompts by parsing its `prompt.json` (one query per component), and evaluate three evaluators: (i) SAM 3 (Carion et al., 2025) concept segmentation, (ii) Grounded-SAM (Ren et al., 2024), and (iii) GPT-4o (Hurst et al., 2024) judging.

For SAM-based methods, a component is considered *recognized* if the method returns at least one valid mask after thresholding; for GPT-4o, recognition is positive if the predicted count is  $> 0$ . We compute precision/recall over component queries, where false positives correspond to recognizing the wrong component (or returning an invalid region), and false negatives correspond to failing to recognize an existing component. The audit shows that VLM judging is more reliable for fine-grained component recognition/counting, whereas SAM 3 remains accurate for extracting step-wise *union foreground* masks. This motivates our hybrid protocol in T2S-CompBench (VLM for semantics; masks for geometry).

Table 5. Pilot audit accuracy (%) on fine-grained component recognition (24 sub-classes, 10 images each).

Method	Precision	Recall	F1-Score
SAM 3 (Text Prompt)	100.00	39.05	56.17
Grounded-SAM	100.00	41.76	58.92
<b>GPT-4o (Ours)</b>	<b>99.51</b>	<b>94.23</b>	<b>96.80</b>

### E.2. GPT-4o Judge: Binary Forcing and Confidence

We use GPT-4o via API with deterministic decoding (temperature = 0) and enforce closed-form outputs: `Yes/No` for semantic questions and `Attached/Detached` for connectivity. We request answer-token log-scores and compute two-way softmax confidence. For a binary decision with answer options  $\{u, v\}$  and corresponding token log-scores  $(\ell_u, \ell_v)$ , we define

$$\text{Conf}_u = \frac{\exp(\ell_u)}{\exp(\ell_u) + \exp(\ell_v)}. \tag{25}$$

To improve parse reliability for counting, we optionally use structured outputs (JSON schema) and extract the integer field count.

### E.3. Instruction Parsing and Metric Definitions (M1–M7)

We parse the goal instruction  $x$  into: required component categories  $\mathcal{C}$  with required counts  $\{N_c^{\text{req}}\}$ , part-bound attribute items  $\mathcal{A}$ , required connectivity pairs  $\mathcal{E}$ , and relation triplets  $\mathcal{R}$ . Unless otherwise specified, semantic/relational metrics are computed by forced-choice GPT-4o judging using Eq. (25) under criteria-based prompt templates (Sec. E.6).

**M1: CN (Component Integrity & Numeracy).** To penalize missing parts and over/under-counting under compositional goals, we score each required category by a scale-invariant count accuracy and then average. Concretely, for each  $c \in \mathcal{C}$  we query GPT-4o to estimate an integer count  $N_c^{\text{pred}}$  and gate by presence  $\text{Recall}_c = \mathbb{I}[N_c^{\text{pred}} > 0]$ , so that a missing required category contributes zero. If present, we assign a per-category score that decays linearly with *relative* count error and is clipped to  $[0, 1]$ :

$$\text{CN} = \frac{1}{|\mathcal{C}|} \sum_{c \in \mathcal{C}} [\text{Recall}_c] \cdot \max\left(0, 1 - \frac{|N_c^{\text{pred}} - N_c^{\text{req}}|}{\max(1, N_c^{\text{req}})}\right). \quad (26)$$

The normalization by  $\max(1, N_c^{\text{req}})$  makes the penalty comparable across categories with different required counts and avoids division by zero, and the outer  $\max(0, \cdot)$  prevents negative scores when the count mismatch is large.

**M2: SF (Shape & Category Fidelity).** To detect failures where parts appear plausible but the overall body shape/category is wrong, we ask a forced Yes/No question  $q_s$  derived from  $x$  and score

$$\text{SF} = \text{Conf}_{\text{Yes}}(q_s). \quad (27)$$

**M3: AF (Attribute Fidelity).** To check part-level attribute binding (e.g., “square handle”, “cylindrical cap”), we ask a forced Yes/No query  $q_a$  for each attribute item  $a \in \mathcal{A}$  and average:

$$\text{AF} = \frac{1}{|\mathcal{A}|} \sum_{a \in \mathcal{A}} \text{Conf}_{\text{Yes}}(q_a), \quad (28)$$

where each  $a$  specifies a target category  $c(a)$  and an attribute; if the target category is missing (i.e.,  $N_{c(a)}^{\text{pred}} = 0$  in CN), we set that term to 0.

**M4: CP (Connectivity Plausibility).** To test whether the object reflects *assembly* rather than a collage of floating parts, we test whether each required connectivity pair  $(A, B) \in \mathcal{E}$  appears attached by a forced Attached/Detached query and compute

$$\text{CP} = \frac{1}{|\mathcal{E}|} \sum_{(A,B) \in \mathcal{E}} \text{Conf}_{\text{Attached}}(A, B). \quad (29)$$

**M5: VT (Visual Topology).** To evaluate spatial relations that require 3D-aware reasoning even under a single canonical view (e.g., above/below/inside/left-of), we ask a forced Yes/No relation query  $q_r$  for each triplet  $r \in \mathcal{R}$  and average:

$$\text{VT} = \frac{1}{|\mathcal{R}|} \sum_{r \in \mathcal{R}} \text{Conf}_{\text{Yes}}(q_r). \quad (30)$$

Each  $r$  encodes a relation (subject, predicate, object) parsed from  $x$ .

**M6: TS (Trace Stability).** To quantify unintended global re-drawing or geometric drift across steps, we measure how much of the previously visible structure is preserved after each incremental update. Let  $M^{(n)}$  be the SAM 3 *union* foreground mask extracted from step image  $v_n$  (front view), which approximates the visible silhouette of the cumulative assembly structure at step  $n$ . We compute step-wise retention of the previous silhouette and average across steps:

$$\text{TS} = \frac{1}{N-1} \sum_{n=2}^N \frac{|M^{(n)} \cap M^{(n-1)}|}{\max(1, |M^{(n-1)}|)}, \quad (31)$$

where  $|\cdot|$  denotes pixel area.

**M7: RA (Step-wise Rationale Alignment).** To evaluate whether each rationale  $z_n$  explains the main visual change from  $v_{n-1}$  to  $v_n$ , we construct a forced Yes/No question  $q_n$  from `step_n.json` (the intended newly added leaf part and its attachment), query GPT-4o on the image pair  $(v_{n-1}, v_n)$ , and average:

$$\text{RA} = \frac{1}{N-1} \sum_{n=2}^N \text{Conf}_{\text{Yes}}(q_n). \quad (32)$$

#### E.4. Multi-view Aggregation Protocol (T2S-CompBench-MV)

**Views.** When multi-view predictions are available, we evaluate four fixed views  $\mathcal{V} = \{\text{front}, \text{left}, \text{right}, \text{back}\}$ . For each metric  $m$  and view  $v \in \mathcal{V}$ , we compute a view-wise score  $m^{(v)}$  using the same procedure as the single-view setting, but feeding the corresponding view image(s).

**Aggregation.** We adopt a view-aggregation rule that distinguishes *visibility-sensitive* metrics from *global-consistency* metrics:

$$\begin{aligned} m^{\text{MV}} &= \max_{v \in \mathcal{V}} m^{(v)}, & m \in \{\text{CN}, \text{AF}, \text{CP}\}, \\ m^{\text{MV}} &= \frac{1}{|\mathcal{V}|} \sum_{v \in \mathcal{V}} m^{(v)}, & m \in \{\text{SF}, \text{VT}, \text{TS}, \text{RA}\}. \end{aligned} \quad (33)$$

**Why max for CN/AF/CP (presence-sensitive).** These metrics depend on whether a *specific component* (and its local property/attachment) is *visible* in a 2D projection. Occlusion and foreshortening can induce false negatives in a single view, while multi-view observations provide redundancy and mitigate occlusion failures. (Xie et al., 2025; Asim et al., 2025) **CN (counting / recall).** Consider a sword: in a side view the blade may collapse to a thin line, causing the judge to output  $N_{\text{blade}}^{(\text{side})} = 0$  and thus  $\text{CN}^{(\text{side})} = 0$ . Max-pooling implements an “exist-if-visible-anywhere” rule:  $\max(\text{CN}^{(\text{front})}, \text{CN}^{(\text{side})})$  restores the correct presence and avoids occlusion-induced false negatives. **AF (part-bound attributes).** Attributes such as “square handle” are only verifiable when the target part is visible with sufficient shape evidence; max-pooling prevents penalizing a correct attribute simply because the part is self-occluded in one view. **CP (connectivity).** Whether two parts appear attached is also visibility-dependent (the contact region may be hidden in a given view); max-pooling avoids spurious “Detached” decisions caused by view-specific occlusion.

**Why mean for SF/VT/TS/RA (global consistency).** These metrics are intended to capture *view-consistent 3D plausibility* rather than view-specific visibility. Recent multi-view generation benchmarks and metrics emphasize that 3D consistency across views is a central requirement for geometry-aware generation. (Xie et al., 2025; Asim et al., 2025; He et al., 2023) Mean aggregation penalizes “view-inconsistent” artifacts that can look correct from one view but fail from others. **SF (global body shape).** A model should not satisfy the shape scaffold only from a single view; averaging encourages a body geometry that remains plausible under viewpoint change. **VT (spatial relations).** Relations like `on-top-of` can be ambiguous in a single 2D projection (e.g., due to perspective overlap). Averaging over multiple views approximates multi-angle sampling of the underlying 3D relation: to achieve a high mean score, the relation must be consistently supported across viewpoints, reducing projection ambiguity. **TS (trace stability).** Mean aggregation is crucial to penalize “billboard / paper-thin” failures: an object may appear stable from `front` (high  $\text{TS}^{(\text{front})}$ ) but collapse or deform under `side` (low  $\text{TS}^{(\text{side})}$ ). The mean yields a medium score, exposing view inconsistency, which is widely recognized as a key failure mode in multi-view/3D generation. (Xie et al., 2025) **RA (step-wise rationale alignment).** If the step rationale describes a 3D-consistent structural constraints addition, the *main change* should be coherent across views over the trace. Mean aggregation discourages view-specific hallucinated edits (e.g., a part appears only in one view) and rewards step-wise changes that remain explainable under viewpoint change.

#### E.5. M1 (CN): Per-category Counting Prompts

For each required category  $c$ , we query GPT-4o *separately* to avoid cross-category interference. We constrain the output to an integer (or JSON `{count: k}`). If the response is invalid, we re-ask with an explicit format reminder and take the first valid output. We use the resulting  $N_c^{\text{pred}}$  to compute CN in Eq. (26).

### E.6. M2–M5: Rigorous Criteria-Based Prompt Templates

Inspired by the rigorous protocol of T2I-CompBench++ (Huang et al., 2025), we adopt a **criteria-based prompting strategy**. Instead of open-ended queries, we provide the evaluator with explicit definitions of positive and negative classes to standardize the decision boundary. All evaluations share a common system prompt to establish the auditing persona.

We provide the detailed prompt templates for the System Prompt and Metrics M2–M5 in Appendix K.3, including:

- **M2 (SF):** Topology audit for global shape matching
- **M3 (AF):** Local property verification for part-bound attributes
- **M4 (CP):** Physical assembly audit for connectivity validation
- **M5 (VT):** 3D spatial reasoning for relation verification

### E.7. M6 (TS): Step-wise Union Foreground Masks with SAM 3

We extract a union foreground mask  $M^{(n)}$  from each step image  $v_n$  using SAM 3. Since fine-grained part classification is unreliable in our domain, we do not require part-level masks for TS. When multiple masks are produced, we take the union of masks with confidence above a fixed threshold and (optionally) keep the largest connected component as the main object mask. We compute TS as the mean retention ratio in Eq. (31), which measures how much of the previous mask is preserved by the current mask.

### E.8. M7 (RA): Step-wise Faithfulness Questions

Let  $z_n$  be the rationale in `step_n.json`. We query GPT-4o with the image pair  $(v_{n-1}, v_n)$  and ask whether the *main* visual change is adding the component/action described by  $z_n$ . We force a Yes/No answer and compute  $\text{Conf}_{\text{Yes}}(q_n)$  for RA in Eq. (32).

## F. Human Evaluation

We conducted human evaluation via Wen JuanXing (WJX). For each test prompt, annotators were asked to rate the generated results on three aspects: *Visual Quality*, *Structural Correctness*, and *Progressive Assembly Logic*. Figure 8, 9, 10, 11, 12, 13 shows the interface used for human evaluation. We randomly sample 50 test prompts stratified by object category. For each prompt, we present outputs from different methods in a blind and randomized order (method identity hidden), and collect 3 independent ratings per method by randomly drawing annotators from the pool. In total, we gather 1050 prompt–output rating instances for human evaluation. Each prompt–output pair is rated by 3 annotators with a score from 1 to 5 for each aspect. Each aspect is rated independently on a 5-point scale: (1) completely not satisfied; (2) partially satisfied; (3) roughly satisfied ( $\sim 50\%$ ); (4) largely satisfied; (5) fully satisfied. We recruited 50 paid annotators. Annotators are paid 0.5 RMB per image evaluated (per final output), and we spend 800 RMB in total on participant compensation.

## Shape of Thought: Progressive Object Assembly via Visual Chain-of-Thought

---

Text prompt: **Construct a compact round planter with a sturdy cylindrical base filled with soil, topped by tall, slender leaves extending upward in a clustered arrangement.**

Generate image:



Rate the matching degree of *Visual Quality*, *Structural Correctness*, and *Progressive Assembly Logic* between the Image and Text Prompt

- 5 - Fully satisfied** : means fully aligned with the prompt/criterion
- 4 - Largely satisfied** : means largely aligned with minor issues
- 3 - Roughly satisfied (~50%)** : means partially aligned
- 2 - Partially satisfied** : means mostly misaligned
- 1 - Completely not satisfied** : means almost irrelevant

Figure 8. WJX interface for the image-text alignment evaluation on SoT (Vase).

Text prompt: **Construct a sleek, S-shaped chair with a continuous curved base forming a seamless transition into the seat and back, featuring a single smooth surface design without visible joints or separations.**

Generate image:



Rate the matching degree of *Visual Quality*, *Structural Correctness*, and *Progressive Assembly Logic* between the Image and Text Prompt

- 5 - Fully satisfied** : means fully aligned with the prompt/criterion
- 4 - Largely satisfied** : means largely aligned with minor issues
- 3 - Roughly satisfied (~50%)** : means partially aligned
- 2 - Partially satisfied** : means mostly misaligned
- 1 - Completely not satisfied** : means almost irrelevant

Figure 9. WJX interface for the image-text alignment evaluation on SoT (Chair).



## Shape of Thought: Progressive Object Assembly via Visual Chain-of-Thought

---

Text prompt: **Construct a modern faucet with an angular, L-shaped spout, mounted on a rectangular base, featuring two hexagonal switches on either side of the spout for controlling water flow.**

Generate image:



Rate the matching degree of **Visual Quality**, **Structural Correctness**, and **Progressive Assembly Logic** between the Image and Text Prompt

- 5 - Fully satisfied** : means fully aligned with the prompt/criterion
- 4 - Highly satisfied** : means largely aligned with minor issues
- 3 - Moderately satisfied** : means partially aligned
- 2 - Slightly satisfied** : means mostly misaligned
- 1 - Not satisfied** : means almost irrelevant

Figure 10. WJX interface for the image-text alignment evaluation on Meshy6 (Faucet).

Text prompt: **Construct a modern, minimalist chair featuring a continuous S-shaped form with a single surface seat seamlessly connecting to a vertically aligned backrest, both supported by a flat, rectangular base.**

Generate image:



Rate the matching degree of **Visual Quality**, **Structural Correctness**, and **Progressive Assembly Logic** between the Image and Text Prompt

- 5 - Fully satisfied** : means fully aligned with the prompt/criterion
- 4 - Largely satisfied** : means largely aligned with minor issues
- 3 - Roughly satisfied (~50%)** : means partially aligned
- 2 - Partially satisfied** : means mostly misaligned
- 1 - Completely not satisfied** : means almost irrelevant

Figure 11. WJX interface for the image-text alignment evaluation on SoT (Chair).

## Shape of Thought: Progressive Object Assembly via Visual Chain-of-Thought

---

Text prompt: **Construct a rectangular ping pong table featuring a smooth, flat tabletop surface with a centered net divider, supported by four tapered legs connected by bar stretchers for stability.**

Generate image:



Rate the matching degree of **Visual Quality**, **Structural Correctness**, and **Progressive Assembly Logic** between the Image and Text Prompt

- 5 - Fully satisfied** : means fully aligned with the prompt/criterion
- 4 - Largely satisfied** : means largely aligned with minor issues
- 3 - Roughly satisfied (~50%)** : means partially aligned
- 2 - Partially satisfied** : means mostly misaligned
- 1 - Completely not satisfied** : means almost irrelevant

*Figure 12.* WJX interface for the image-text alignment evaluation on SoT (Table).

Text prompt: **Construct a spherical lamp cover featuring evenly spaced vertical slats curving outward from a narrow top rim to a wider open base, creating a cage-like structure.**

Generate image:



Rate the matching degree of **Visual Quality**, **Structural Correctness**, and **Progressive Assembly Logic** between the Image and Text Prompt

- 5 - Fully satisfied** : means fully aligned with the prompt/criterion
- 4 - Largely satisfied** : means largely aligned with minor issues
- 3 - Roughly satisfied (~50%)** : means partially aligned
- 2 - Partially satisfied** : means mostly misaligned
- 1 - Completely not satisfied** : means almost irrelevant

*Figure 13.* WJX interface for the image-text alignment evaluation on Bagel (Lamp).

Table 6. Qwen re-audit setup for judge consistency.

Item	Value
Primary judge	GPT-4o
Alternative judge	Qwen2-VL-7B-Instruct
Subset sampling	$N_{\text{sub}} = 200$ prompts, stratified by category
Judged metrics	CN/SF/AF/CP/VT/RA (TS is mask-based)
Binary forcing	Yes/No; Attached/Detached
Confidence (Qwen)	self-consistency voting ( $R = 5$ )
Uncertainty	95% CI via prompt-level bootstrap

**Aggregation and uncertainty.** We first average the 3 ratings per prompt to obtain a prompt-level score, and then report the mean across prompts. We additionally report **mean  $\pm$  95% CI** computed via **prompt-level bootstrap**: we resample prompts with replacement, recompute the mean, and take the 2.5/97.5 percentiles as the 95% CI.

**Inter-annotator agreement.** We compute **Fleiss’  $\kappa$**  separately for each aspect by treating the 5-point ratings as categorical labels with  $n = 3$  raters per prompt.

### G. Judge Diversity and Consistency

**Motivation.** VLM-as-a-judge may introduce model-specific biases. We therefore validate the robustness of T2S-CompBench by re-auditing a stratified subset with an alternative open-weight VLM judge and quantifying cross-judge consistency.

**Judges.** Our primary judge is GPT-4o (Sec. E.2). We additionally use **Qwen2-VL-7B-Instruct** as an alternative multimodal judge.

**Subset and protocol.** We sample  $N_{\text{sub}}=200$  test prompts stratified by object category. For each prompt, we re-run the judge-based metrics **CN/SF/AF/CP/VT/RA** on the corresponding rendered outputs (using the identical prompt templates and forced-choice formats). Metric **TS** is mask-based (SAM 3) and thus judge-independent.

**Closed-form outputs and confidence.** For binary questions (SF/AF/VT/RA: Yes/No; CP: Attached/Detached), we enforce closed-form outputs with deterministic decoding. As Qwen2-VL local inference does not reliably expose answer-token log-scores, we approximate confidence by **self-consistency voting**: repeat each query  $R=5$  times (temperature = 0.2, top- $p = 0.9$ ) and define  $\widehat{\text{Conf}}_{\text{yes}} = \frac{1}{R} \sum_{r=1}^R \mathbb{I}[\text{Yes}]$  (and similarly for Attached). We use the same confidence definition for GPT-4o by mapping its forced-choice output to  $\{0, 1\}$  when computing agreement; score-level correlations use confidence-like scores in  $[0, 1]$ .

**Consistency metrics.** Let  $s_i^{(a)}$  be the per-sample score from judge  $a$  for a given metric. We report: (i) **score correlation** (Spearman  $\rho$ , Kendall  $\tau$ ) between  $\{s_i^{(\text{GPT-4o})}\}$  and  $\{s_i^{(\text{Qwen})}\}$ ; (ii) **binary decision agreement** by thresholding at 0.5 to get  $y_i \in \{0, 1\}$ , then reporting raw agreement and Cohen’s  $\kappa$ ; (iii) **method-level ranking stability** by ranking methods using subset-level mean scores and reporting Kendall  $\tau$  between rankings as well as the top-1 match rate. All statistics are reported with **95% CIs** via bootstrap resampling over prompts (2.5/97.5 percentiles).

**Qualitative disagreement audit.** To diagnose systematic judge differences, we further inspect the top-10 prompts with the largest absolute score gaps  $|s_i^{(\text{GPT-4o})} - s_i^{(\text{Qwen})}|$  per metric and categorize failure modes (e.g., occlusion sensitivity for CN/AF/CP, ambiguous projection for VT, and small-step edits for RA). We will release these cases and the corresponding judge transcripts for transparency.

Table 7. Cross-judge consistency on the stratified subset.

Metric	Spearman $\rho$ $\uparrow$	Kendall $\tau$ $\uparrow$	Agree (%) $\uparrow$	Cohen $\kappa$ $\uparrow$	95% CI
CN	0.65	0.51	74.5	0.48	$\pm 0.09$
SF	0.84	0.68	88.0	0.69	$\pm 0.06$
AF	0.76	0.59	81.2	0.58	$\pm 0.07$
CP	0.72	0.56	77.4	0.53	$\pm 0.08$
VT	0.69	0.53	75.8	0.50	$\pm 0.08$
RA	0.79	0.62	83.6	0.61	$\pm 0.06$
<b>Method ranking</b>	Rank $\tau$ : 0.86		Top-1 Match: 100%		–

## H. Limitations

**Failure cases.** As shown in figure 14, we show representative failure examples where SoT produces globally coherent assemblies but still misses small or thin components. These errors are most prominent when the missing parts are partially or fully occluded in the canonical front view, or when they project to sub-pixel / low-contrast regions. This suggests that single-view rendered supervision can under-specify occluded geometry: the model may satisfy the observed 2D evidence while failing to recover hidden details, leading to residual part omissions despite correct high-level topology.



(a) Case A: The model did not generate the base of the display.

(b) Case B: The model generated an incorrect shape due to the occlusion.

Figure 14. Examples of cases where the discovered structural tasks failed to be executed properly or details were omitted.

**Viewpoint and Modality Constraints.** Our supervision is currently centered on a canonical front view, a choice dictated by the prohibitive computational cost of dense visual traces (which already saturate  $32 \times H100$  GPUs in the single-view setting). Naively scaling to multi-view supervision would multiply visual token consumption and training time, rendering it infeasible under current constraints. **Crucially, however,** our ecosystem is fully ready for this extension: the SoT-26K dataset already includes auxiliary multi-view renderings (left/right/back), our codebase supports multi-stream data loading, and the T2S-CompBench benchmark is established with a rigorous multi-view aggregation protocol. We identify compute-efficient strategies—such as stochastic view sampling or latent distillation—as the immediate next step to unlock this capability within our established infrastructure.

**Evaluation and Metric Biases.** Our benchmark relies on a hybrid automatic evaluator, where semantic/relational metrics are judged by a closed-source VLM (GPT-4o) and trace stability uses segmentation masks from SAM. While we include a re-audit with an open-weight judge and enforce closed-form decisions, VLM-as-a-judge can still be sensitive to prompt design, model updates, and inherent scoring biases, which may affect absolute scores and reproducibility.

**Data and Taxonomy Bias.** SoT-26K is derived from PartNet CAD assets and rendered synthetically with an enforced leaf-part-per-step schedule; this introduces domain and taxonomy bias (limited object categories and annotation conventions) and may not reflect real-world assembly granularity where multiple parts can be installed jointly.

**Future Directions.** Future work may prioritize compute-efficient training, stronger multi-view robustness, more transparent evaluation alternatives, and broader data coverage. Specifically: (i) **Geometry and Physics Priors:** To reduce the uncertainty of implicitly learning “shape” from 2D trajectories, differentiable rendering regularizers and simulation-inspired constraints (e.g., stability, non-interpenetration) can be introduced. (ii) **Multi-view Framework:** A multi-view training framework can be incorporated by jointly supervising intermediate states under multiple cameras to encourage cross-view consistency. (iii) **Efficiency:** Addressing the cost of multi-view supervision via compute-aware view sampling (e.g., view dropout) or shared-state caching. (iv) **Data Diversity:** Broadening coverage beyond PartNet by incorporating diverse large-scale 3D assets to enable more varied assembly behaviors.

## I. Qualitative Demonstration: From SoT Traces to 3D Meshes

While Shape-of-Thought (SoT) primarily operates in the rendered 2D domain to internalize assembly logic, a key question remains: does the model learn true 3D structural constraints, or merely 2D visual mimicry? To validate the **geometric rationality** of our generated traces, we provide a qualitative proof-of-concept by “lifting” our 2D outputs into 3D meshes.

We utilize an off-the-shelf mask-to-3D pipeline (specifically SAM 3D (Team et al., 2025)) to process the final generated view  $v_N$  from our SoT model. As illustrated in Figure 15, the results show that SoT outputs can be reconstructed into coherent 3D meshes.

It is important to emphasize that this successful reconstruction is not primarily due to the capability of the lifting tool, but rather a direct consequence of the **structural clarity** and **distinct part segmentation** inherent in the SoT generation process. Unlike standard text-to-image models that often produce geometrically ambiguous textures or “dream-like” artifacts, SoT’s visual chain-of-thought shows that:

- Component boundaries are sharp and explicitly defined (as shown in the segmentation map in Figure 15, Left).
- The connectivity between parts (e.g., the stem connecting to the lamp shades) respects physical plausibility.
- The spatial layout is consistent enough to support depth estimation and mesh extraction.

Therefore, the fact that a straightforward, inference-only lifting tool can derive clean 3D topology from our 2D traces serves as a qualitative proxy suggesting SoT captures some geometric regularities that support 3D-consistent composition.

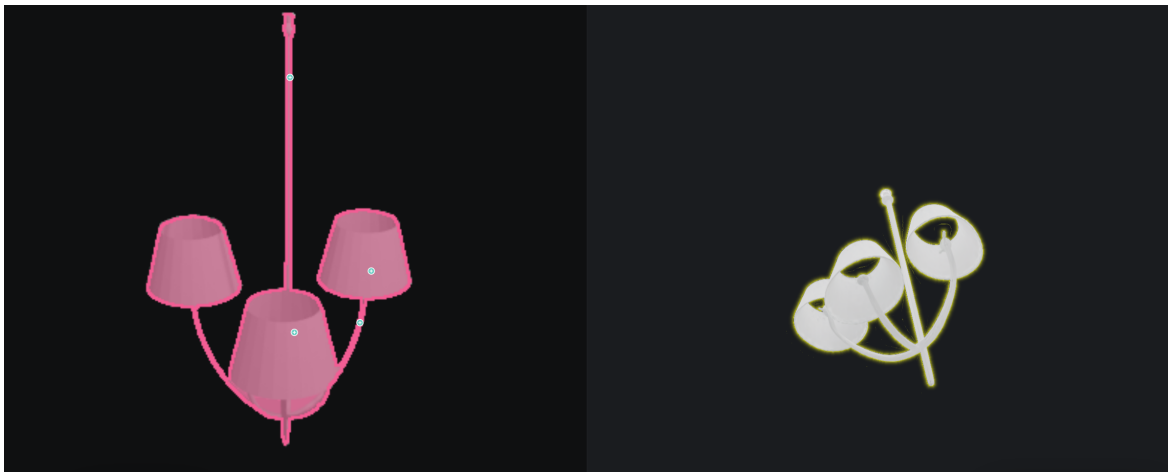


Figure 15. **Qualitative 3D Lifting.** Left: The generated image from SoT exhibits clear structural boundaries and distinct part separation (visualized via SAM masks). Right: The resulting 3D mesh lifted using SAM 3D. The successful reconstruction verifies that SoT traces possess the necessary geometric integrity and component distinctness to support downstream 3D applications.

**Dependency on Downstream Lifting Tools.** While SoT provides a geometrically consistent visual signal, the fidelity of the final 3D mesh is inevitably bounded by the capabilities of the downstream lifting tool. As shown in Figure 16, SAM 3D can capture fine-grained geometries in structurally prominent cases, such as the intertwined tentacles on the sword hilt



Figure 16. **Diverse Qualitative 3D Lifting Results.** We visualize the SoT generated segmentation masks (Left, pink) and the corresponding 3D meshes lifted via SAM 3D (Right, gray) across various categories. The results highlight SoT’s ability to maintain geometric rationality across varying complexities. Note that while the lifting pipeline reconstructs complex organic shapes like the *sword’s tentacles*, it may smooth out high-frequency details like the *keyboard keys* due to resolution constraints, despite these structures being explicitly segmented in the SoT source mask.

and the engraved patterns on the blade. However, limitations persist in handling high-frequency repetitive structures. For instance, in the keyboard case (top right), although SoT explicitly generates and segments the individual keys (clearly visible in the pink segmentation mask), the current SAM 3D pipeline tends to smooth these discrete details into a flat surface. This discrepancy highlights a critical distinction: **SoT captures the semantic and structural logic** (knowing there should be individual keys and placing them correctly), whereas the loss of detail is merely a reconstruction artifact of the specific lifter used. This suggests that the *visual information* provided by SoT is sufficiently rich, and as image-to-3D lifting techniques such as LRM (Hong et al., 2024) continue to evolve, the 3D quality derived from SoT traces will naturally improve without architectural changes to SoT itself.

## J. Additional Qualitative Results by Category

We provide a comprehensive gallery of generation traces across five distinct object categories: **Dining & Tableware**, **Electronics & Office**, **Furniture & Infrastructure**, **Kitchenware & Appliances**, and **Lifestyle & Accessories**.

These examples further demonstrate Shape-of-Thought’s capability to:

- Handle diverse geometries, from organic curves (e.g., bowls, plants) to rigid mechanical structures (e.g., keyboards, appliances).
- Maintain strict structural logic, forcing parts are connected plausibly (e.g., table legs attached to corners, handles attached to doors).
- Execute fine-grained attribute binding, such as placing specific numbers of keys or generating specific handle shapes as

requested in the prompts.







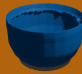



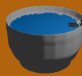

Dining & Tableware			
<p><b>Prompt:</b> Construct ...bottle with a ... body... a narrow neck, featuring...</p>	<p><b>Prompt:</b> Construct a ... dagger featuring ... blade ... handle ... guard ...butt...</p>	<p><b>Prompt:</b> Construct a rounded bowl featuring ... body with ...</p>	<p><b>Prompt:</b> Construct a ... mug featuring ... handle ... containing liquids.</p>
<p><b>Step 1</b></p> <p>First, construct the smooth cylindrical body of the bottle, ensuring it is tall and slender.</p> 	<p><b>Step 1</b></p> <p>First, attach the wide guard centrally, ensuring it features protruding ends that extend outward.</p> 	<p><b>Step 1</b></p> <p>First, create a solid, circular base for the bowl.</p> 	<p><b>Step 1</b></p> <p>First, construct a cylindrical body with a vertically ribbed texture and a hollow interior.</p> 
<p><b>Step 2</b></p> <p>Next, attach the narrow neck to the top of the smooth cylindrical body, ensuring it tapers seamlessly from the wider base to create a slender and elongated profile.</p> 	<p><b>Step 2</b></p> <p>Next, attach the slim cylindrical handle vertically below the wide guard, ensuring it aligns centrally for balance and grip.</p> 	<p><b>Step 2</b></p> <p>Next, attach the smooth curved body with an indented section along the rim seamlessly to the bottom.</p> 	<p><b>Step 2</b></p> <p>Next, attach the curved handle to the side of the cylindrical body.</p> 
<p><b>Step 3</b></p> <p>Finally, attach the flat lid seamlessly atop the narrow neck of the bottle, ensuring it aligns perfectly with the cylindrical shape to maintain a smooth, continuous form.</p> 	<p><b>Step 3</b></p> <p>Now, attach the rounded butt to the base of the slim cylindrical handle.</p> 	<p><b>Step 3</b></p> <p>Finally, incorporate the uniquely indented section along the rim, seamlessly attached to the interior for containing items.</p> 	<p><b>Step 3</b></p> <p>Finally, ensure the interior is hollow to accommodate liquids.</p> 

Figure 17. **Category: Dining & Tableware.** The model generates hollow structures (e.g., the interior of the mug and bowl) and handles complex curvatures in objects like the dagger and bottle, maintaining smooth topological transitions.

**Kitchenware & Appliances**






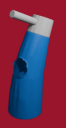
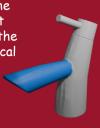






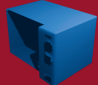
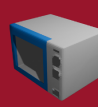
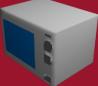
<p><b>Prompt:</b> Construct a tall, rectangular trashcan with ... featuring ...</p> <p><b>Step 1</b></p> <p>First, position the wide, rectangular container bottom flat on the surface.</p>  <p><b>Step 2</b></p> <p>Next, position the tall rectangular container box directly above the wide container bottom.</p>  <p><b>Step 3</b></p> <p>Then, position the flat, detachable cover lid centrally on top of the container box, featuring a central handle.</p>  <p><b>Step 4</b></p> <p>Finally, attach the slightly tapered container neck between the cover lid and the container box.</p> 	<p><b>Prompt:</b> Build a modern cylindrical faucet featuring ... extending ...</p> <p><b>Step 1</b></p> <p>First, position the thin cylindrical switch horizontally on top.</p>  <p><b>Step 2</b></p> <p>Next, position the sleek vertical support centrally, forming the main body of the faucet.</p>  <p><b>Step 3</b></p> <p>Finally, attach the short, wide spout extending from the side of the vertical support.</p> 	<p><b>Prompt:</b> Construct a compact rectangular dishwasher with a flat frame ...</p> <p><b>Step 1</b></p> <p>First, construct a compact rectangular frame with a smooth, flat surface.</p>  <p><b>Step 2</b></p> <p>Next, attach the protruding door frame to the front of the smooth, flat frame.</p>  <p><b>Step 3</b></p> <p>Finally, attach the long horizontal handle centrally on the front panel of the protruding door frame.</p> 	<p><b>Prompt:</b> Construct a tall, rectangular refrigerator with ... featuring ...</p> <p><b>Step 1</b></p> <p>First, construct a tall, rectangular frame with smooth, rounded edges.</p>  <p><b>Step 2</b></p> <p>Next, add the seamless door frame, aligning it vertically and smoothly around the tall, rectangular structure.</p>  <p><b>Step 3</b></p> <p>Finally, attach the short, horizontal handle centrally on the side of the door.</p> 	<p><b>Prompt:</b> Construct a rectangular microwave with flat ... featuring ...</p> <p><b>Step 1</b></p> <p>First, construct the solid outer frame with a rectangular shape and smooth surfaces.</p>  <p><b>Step 2</b></p> <p>Next, attach the prominent door frame centrally, featuring a glass panel enclosed within the sturdy door frame.</p>  <p><b>Step 3</b></p> <p>Finally, insert the short, glass panel centrally within the sturdy door frame.</p> 
---	---	---	---	---

Figure 18. **Category: Kitchenware & Appliances.** Showcasing the assembly of multi-part mechanical objects. The traces exhibit correct part-whole relationships, such as fitting doors onto frames and attaching handles to specific panels.

**Lifestyle & Accessories**






<p><b>Prompt:</b> Construct ... scissors featuring ... blades with ... pivot point, and ...</p> <p><b>Step 1</b></p> <p>First, add the blade, positioning it horizontally to form the initial cutting edge of the scissors.</p>  <p><b>Step 2</b></p> <p>Then, add the second blade parallel to the first blade, ensuring they intersect at the pivot point.</p>  <p><b>Step 3</b></p> <p>Now, attach the handle to the base of the blades, ensuring it wraps around and secures them at the pivot point.</p>  <p><b>Step 4</b></p> <p>Finally, attach the second handle on the opposite side of the existing handle, aligning it with the blade to complete the structure.</p> 	<p><b>Prompt:</b> Construct a rounded planter featuring ... soil with ... leaves.</p> <p><b>Step 1</b></p> <p>First, position the compact round planter with a sturdy cylindrical base.</p>  <p><b>Step 2</b></p> <p>Next, fill the sturdy cylindrical base with soil, ensuring it is level with the planter's rim.</p>  <p><b>Step 3</b></p> <p>Finally, position the tall, slender leaves in a clustered arrangement extending upward from the soil.</p> 	<p><b>Prompt:</b> Construct a rounded cap featuring ... dome-shaped top with ...</p> <p><b>Step 1</b></p> <p>First, add the wide and flat curved bill extending from the front.</p>  <p><b>Step 2</b></p> <p>Next, position the smooth dome-shaped top centrally above the bill.</p>  <p><b>Step 3</b></p> <p>Finally, position the small circular button centrally on the dome-shaped top panel.</p> 	<p><b>Prompt:</b> Create a ... bag with ... body and two parallel, curved handles ...</p> <p><b>Step 1</b></p> <p>First, construct the solid, blocky body of the bag with a rectangular shape.</p>  <p><b>Step 2</b></p> <p>Next, attach a single curved handle to the top of the solid, blocky body.</p>  <p><b>Step 3</b></p> <p>Finally, attach the second curved handle parallel to the first, emerging from the top of the solid, blocky bag body.</p> 	<p><b>Prompt:</b> Construct ... desk lamp featuring a wide, faceted lamp shade ...</p> <p><b>Step 1</b></p> <p>First, position the hexagonal base centrally.</p>  <p><b>Step 2</b></p> <p>Next, attach the dual-straight-bar arm vertically to the center of the hexagonal base.</p>  <p><b>Step 3</b></p> <p>Then, attach the second straight bar horizontally to the top of the existing vertical bar.</p>  <p><b>Step 4</b></p> <p>Finally, attach the wide, faceted lamp shade to the top of the dual-straight-bar arm.</p> 
--	--	---	---	--

Figure 19. **Category: Lifestyle & Accessories.** Examples of diverse object topologies. The model handles thin structures (scissors blades), organic arrangements (planter leaves), and curved surfaces (cap bill) with high fidelity to the textual attributes.





Figure 20. Category: Electronics & Office. Demonstrating precision in component placement and numeracy. Note the grid-aligned generation of keyboard keys and the structural articulation of the laptop hinge and headphone band.

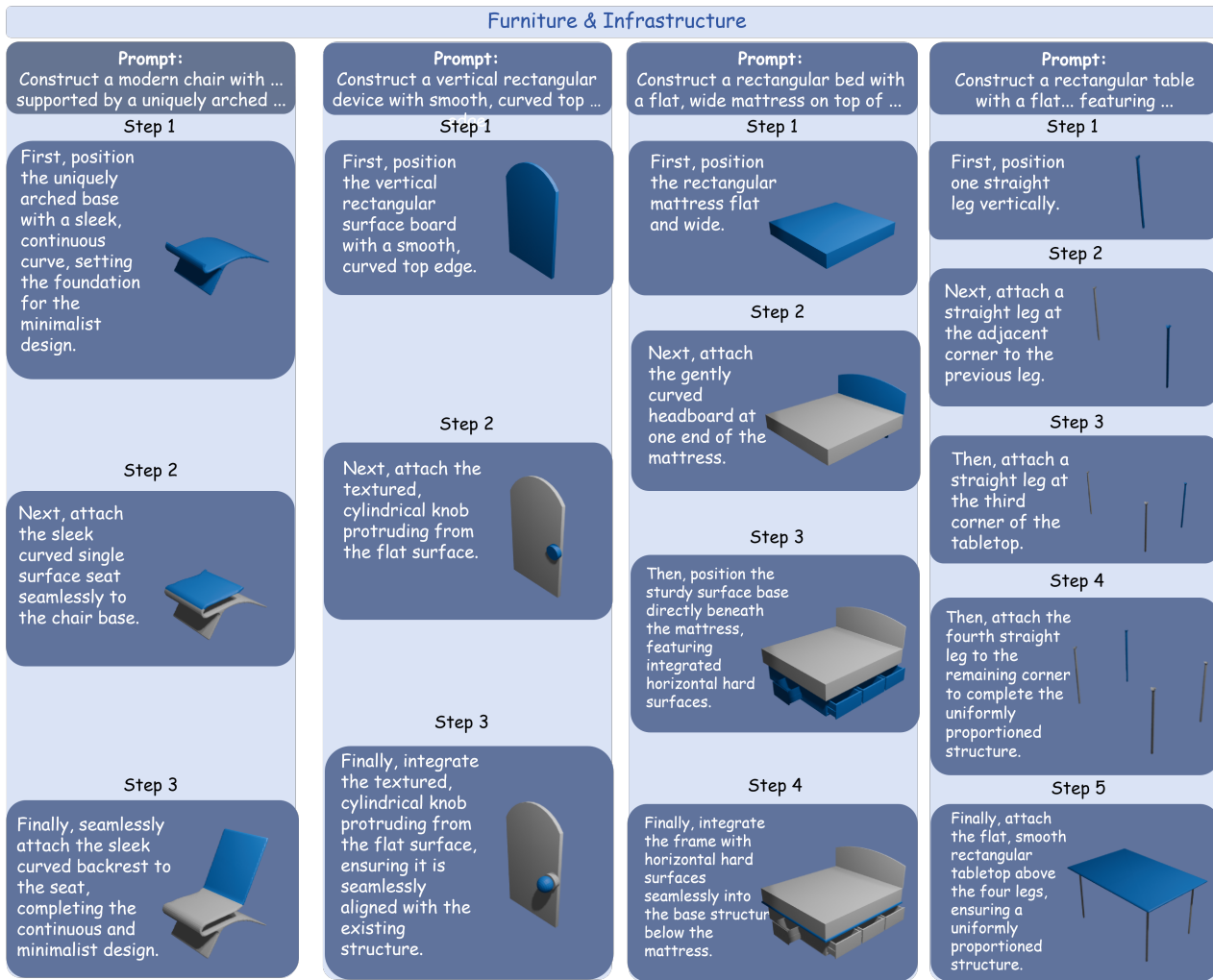


Figure 21. Category: Furniture & Infrastructure. Highlighting structural stability and spatial reasoning. The model correctly positions support structures (legs, bases) relative to the main surfaces (tabletops, seats) to ensure physical plausibility.

## K. Prompt Templates

This appendix provides the detailed prompt templates used for generating multimodal annotations in the SoT dataset construction pipeline.

### K.1. CoT Generation Template

The following template is used to generate step-by-step reasoning traces for 3D object assembly:

#### CoT Generation Template

You are an expert at describing the progressive construction of 3D objects  
↪ with focus on essential shape and positional details.

Your task is to generate concise descriptions for each step in building a 3D  
↪ object, including only the most critical information needed for 3D  
↪ generation.

Guidelines:

1. Describe what new parts are added in this step and their key  
↪ characteristics.
2. Focus ONLY on essential details from the prompt:
  - Shape and geometry (rectangular, curved, tapered, straight, ornate)
  - Design features (engraved patterns, complex guard, intertwined  
↪ tentacles)
  - Key positions and alignments (centrally, above, below, attached to)
3. Use clear, direct language without redundant explanations or purpose  
↪ statements.
4. Begin with an appropriate transition word based on the step number and  
↪ total steps:
  - Single step (1/1): No transition word needed - describe directly
  - Step 1 (multi-step): "First"
  - Step 2: "Next"
  - Middle steps: "Then"
  - Final step: "Finally"
5. Keep descriptions extremely concise - focus only on shape, design, and  
↪ position.
6. Output only the description text - no step numbers, prefixes, or  
↪ formatting markers.
7. Avoid any explanatory phrases about stability, foundation, or future  
↪ components.

Example outputs for a sword:

First, position the complex guard centrally, designed to resemble  
↪ intertwined tentacles.

Next, attach the slim handle directly below the complex guard.

Then, attach the rounded butt to the end of the slim handle.

Finally, attach the straight, tapered blade above the complex guard.

Example outputs for a suitcase:

First, position the tall rectangular bag body upright with rounded edges.

Next, attach the extended vertical handle centrally to the top of the bag  
↪ body.

Finally, add the sturdy base with subtle feet underneath the bag body.

Generate a concise description for Step {step\_number} of {total\_steps} in  
↪ building a {object\_type}.

Object Description (from prompt):  
{prompt\_text}

Existing parts (already added):  
{existing\_parts}

New parts added in this step:  
{new\_parts}

Important notes:

- This is step {step\_number} of {total\_steps}.
- {step\_note}
- Focus ONLY on essential shape, design features, and positional details.
- Keep extremely concise - only include information critical for 3D  
↪ generation.
- Avoid explanatory phrases about stability, foundation, or future  
↪ components.
- Output only the description text, starting directly with the correct  
↪ transition word.

Write the concise description for this step.

## K.2. Goal Prompt Generation Template

The following template is used to generate high-level goal prompts for 3D object construction:

### Goal Prompt Generation Template

You are an expert at describing sequential construction steps for 3D  
↪ objects.

Below is the complete list of final components of the finished 3D object:  
{parts\_text}

{construction\_steps}

{visual\_reference\_note}

Write a highly specific goal prompt describing the final object that should  
↪ be built.

Your prompt MUST:

1. Identify the object category AND clearly specify the unique visual  
↪ characteristics that distinguish it from other similar objects.
2. Use the parts list, construction sequence, AND the image (if available)  
↪ to extract concrete, visible details such as:
  - shape and geometry (curved, straight, rectangular, tapered, wide, thin)
  - proportions (long handle, wide blade, short base, tall body)
  - structural relationships between parts (how they connect/assemble)

- notable design elements (holes, slots, circular guards, angled edges)
  - assembly sequence implications (what gets added first, last, etc.)
  - material cues implied by part names
3. Focus only on describing the final object | not the construction steps.
  4. Be concise but detailed enough that two similar objects produce clearly  
→ different prompts.
  5. Use imperative language ("Build a...", "Create a...", "Construct a...").
  6. Output only the prompt text, with no prefix or explanation.

Below are examples (learn the level of specificity, not the exact wording):

Good Example 1 (specific enough to distinguish objects within the same  
→ category):

- "Create a wide rectangular cleaver with a flat metal blade, a straight  
→ cutting edge, and a short cylindrical wooden handle."

Good Example 2 (another distinct knife example):

- "Build a curved single-edged knife featuring an outward-arching blade, a  
→ sharp pointed tip, and a long wrapped grip."

Good Example 3 (for an object with unique structural elements):

- "Construct a narrow double-edged dagger with a symmetrical tapered blade,  
→ a slightly raised center ridge, and a circular guard attached to a slim  
→ straight handle."

Bad Example (too generic; avoid outputs like this):

- "Build a knife."

Now generate the goal prompt that precisely describes this specific final  
→ object.

### K.3. Evaluation Prompt Templates

The following templates are used for automated evaluation in T2S-CompBench, providing rigorous criteria-based prompts for VLM-based auditing.

#### System Prompt (Audit Persona)

You are an expert 3D geometric auditor. You are evaluating a 2D rendering of  
→ a procedural 3D assembly.  
Your goal is to assess Structural Integrity, Geometric Fidelity, and Spatial  
→ Logic based ONLY on the visual evidence.  
Do not hallucinate obscured parts. Be critical: ambiguous or floating  
→ structures should be penalized.

#### M2: Shape (SF) – Topology Audit

[SYSTEM ROLE]

You are an expert Geometric Topology Auditor. Your task is to perform a  
→ structural integrity check on the primary object in the image against a  
→ specific topological description.

[INPUT]

- Image: [Input Image]
- Target Description: "{SHAPE\_DESCRIPTION}"

[AUDIT PROTOCOL]

Analyze the object following these logical steps:

1. Primitive Abstraction: Ignore textures, colors, and labels. Reduce the  
→ object to its base 3D primitives (e.g., cylinder, cuboid, sphere,  
→ torus).
2. Silhouette & Ratio: Evaluate the global outer boundary. Does the  
→ height-to-width ratio align with the description?
3. Feature Mapping: Identify specific topological markers (e.g., "narrow  
→ waist," "tapered top," "hollow center"). Verify if these are structural  
→ or merely visual artifacts.

[PASS/FAIL CRITERIA]

- PASS (Yes) if:
  1. The base geometric primitive matches the description perfectly.
  2. The aspect ratio and symmetry (if applicable) are consistent with the  
→ target.
  3. All named structural features are clearly articulated and correctly  
→ positioned.
- FAIL (No) if:
  1. Category Mismatch: Base geometry differs (e.g., a rectangular prism  
→ instead of a cylinder).
  2. Structural Collapse: Significant geometric distortion, non-manifold  
→ edges, or unrealistic mesh-like artifacts.
  3. Feature Absence: Defined traits (like the 'narrow waist') are missing  
→ or structurally ambiguous.

[OUTPUT FORMAT]

1. Analysis:
  - Geometry: [Identify base primitive]
  - Silhouette: [Analyze proportions and outline]
  - Key Features: [Confirm presence/absence of specific traits]
2. Final Verdict:
  - Answer: (Yes/No)
  - Confidence Score: (0-100%)

### M3: Attributes (AF) – Local Property Verification

Image: [Input Image]

Task: Verify Local Part Attributes.

Target Part: "{PART\_NAME}"

Target Attribute: "{ATTRIBUTE}" (e.g., "square", "wooden", "transparent")

Instructions:

1. Locate the "{PART\_NAME}". If it is missing, the answer is No.
2. Inspect its visual texture, material, and local geometry.
3. Compare strictly against the attribute "{ATTRIBUTE}".

Question: Is the "{PART\_NAME}" clearly rendered as "{ATTRIBUTE}"?

Answer (Yes/No):

#### M4: Connectivity (CP) – Physical Assembly Audit

[SYSTEM ROLE]

You are a High-Precision Visual Quality Assurance Auditor. Your task is to  
→ verify if a specific sub-component of an object strictly adheres to a  
→ defined material, geometric, or textural attribute.

[INPUT]

- Target Part: "{PART\_NAME}"
- Target Attribute: "{ATTRIBUTE}"

[INSPECTION PROTOCOL]

Conduct the audit using the following multi-modal logic:

1. Spatial Localization: Identify the exact bounding region of the  
→ "{PART\_NAME}". If the part is occluded, missing, or hallucinated, fail  
→ the audit immediately.
2. Material/Texture Decomposition:
  - For Materials (e.g., "wooden"): Look for grain patterns, organic  
→ irregularities, and matte light absorption.
  - For Opticality (e.g., "transparent"): Look for refraction, background  
→ bleed-through, and specular highlights.
  - For Geometry (e.g., "square"): Analyze edge orthogonality (90-degree  
→ angles) and aspect ratio parity.
3. Logical Consistency: Is the attribute physically plausible for the  
→ rendered object, or does it appear as a "texture wrap" on a wrong shape?

[JUDGMENT CRITERIA]

- PASS (Yes): The attribute is unambiguous. The visual evidence (e.g., wood  
→ grain, clear refraction, sharp 90-degree corners) is high-fidelity and  
→ matches the "{ATTRIBUTE}" description perfectly.
- FAIL (No):
  - Presence Check: The "{PART\_NAME}" is missing or unidentifiable.
  - Attribute Mismatch: The part exists but displays a different attribute  
→ (e.g., metallic instead of wooden).
  - Ambiguity: The rendering is too blurry, low-resolution, or distorted  
→ to definitively confirm the attribute.

[OUTPUT FORMAT]

1. Evidence Description: [Describe the visual properties of the {PART\_NAME}  
→ in detail]
2. Discrepancy Check: [List any deviations from the target "{ATTRIBUTE}"]
3. Final Verdict:
  - Answer: (Yes/No)
  - Confidence Score: (0-100%)

#### M5: Topology (VT) – 3D Spatial Reasoning

[SYSTEM ROLE]

## Shape of Thought: Progressive Object Assembly via Visual Chain-of-Thought

You are a 3D Scene Reconstruction Analyst. Your task is to audit the spatial  
↪ relationship between two components by projecting their 2D image  
↪ coordinates into an implied 3D coordinate system.

[INPUT]

- Subject (A): "{PART\_A}"
- Object (B): "{PART\_B}"
- Proposed Relation: "{RELATION}"

[SPATIAL REASONING PROTOCOL]

Perform a volumetric analysis based on the following depth cues:

1. Occlusion & Layering: Does the boundary of {PART\_A} interrupt the surface  
↪ of {PART\_B}? If {PART\_A} is "inserted into" {PART\_B}, identify the  
↪ contact line where the surfaces intersect.
2. Perspective & Vanishing Points: Do the scale and orientation of both  
↪ parts align with a shared 3D perspective? Check if the shadows cast by  
↪ {PART\_A} fall realistically upon {PART\_B}.
3. Contact Points vs. Floating: Look for "contact shadows" (ambient  
↪ occlusion) at the interface. If the relation is "on top of," is there a  
↪ visible compression or shadow indicating physical touch, or is it merely  
↪ "floating" in 2D space?
4. Geometric Logic: Does the 3D volume of {PART\_A} physically fit within or  
↪ around the 3D volume of {PART\_B} without mesh self-intersection?

[JUDGMENT CRITERIA]

- PASS (Yes): The 3D depth cues (shadows, perspective, occlusion)  
↪ consistently support the "{RELATION}" without logical contradiction.
- FAIL (No):
  - 2D Coincidence: The parts overlap in pixels but their depth cues  
↪ suggest they are on different planes (e.g., "floating").
  - Perspective Mismatch: {PART\_A} and {PART\_B} appear to be rendered from  
↪ different camera angles.
  - Physical Impossibility: The parts intersect in a way that violates  
↪ solid geometry (e.g., ghosting or clipping).

[OUTPUT FORMAT]

1. Depth Cue Analysis: [Detail the evidence from shadows, occlusion, and  
↪ perspective]
2. Intersectional Logic: [Describe how the volumes of A and B interact]
3. Final Verdict:
  - Answer: (Yes/No)
  - Confidence Score: (0-100%)

### 3D Visual Testing System Prompt

[ROLE]

You are a Professional 3D Asset Visualizer specialized in Industrial Design  
↪ Clay Rendering. Your goal is to generate high-fidelity, untextured 3D  
↪ model visualizations for geometric topology audits.

[VISUAL STYLE GUIDE]



## Shape of Thought: Progressive Object Assembly via Visual Chain-of-Thought

1. Material: Uniform "Clay" or "Plaster" material. Zero texture, zero color, → zero transparency (unless explicitly requested).
2. Surface: Matte finish with soft Lambertian reflections. Use subtle → Ambient Occlusion (AO) to define edges and contact points.
3. Background: Pure, sterile white (#FFFFFF). No horizon line, no floor → shadows, no environmental distractions.
4. Lighting: Neutral "Studio Lighting." Use a three-point light setup to → create clear highlights and soft shadows that define 3D volume and depth → without blowing out details.
5. Camera: Standard 3/4 perspective or Isometric view. Ensure the primary → object is centered and fills 70-80% of the frame.

### [TECHNICAL CONSTRAINTS]

- NO photorealistic textures (e.g., no wood grain, no brushed metal).
- NO text, logos, or watermarks.
- NO motion blur or depth of field (everything should be in sharp focus).
- NO "painterly" or artistic filters. Maintain clean, hard-surface or → organic CAD-like precision.

### [OUTPUT PROTOCOL]

When given a "{SHAPE\_DESCRIPTION}", render the object strictly following the → clay-style guidelines above. Prioritize the clarity of "junctions," → "seams," and "spatial intersections" between parts.